AN INVESTIGATION INTO THE MAGNETIC PROPERTIES ASSOCIATED WITH THE SPIN CROSSOVER OF Fe(III) COMPOUNDS OF THE FORM [Fe(X)L]A

by

Thomas J. Jewett
B. S., Loras College, 1984

A MASTER'S THESIS

submitted in partial fulfillment of the
requirements for the degree

MASTER OF SCIENCE

Department of Chemistry

KANSAS STATE UNIVERSITY

Manhattan, Kansas

1987

Approved by:

Keith J. Purcell
Major Professor

I would like to dedicate this work to my parents, James and Barbara Jewett for their support throughout both my undergraduate and graduate careers. I would also like to dedicate this work to all those people who made my stay at Kansas State an enjoyable experience and who helped me make it through the hardest part of this work, the rewrites.

Acknowledgements

I would like to thank Drs. Basil Curnutte and John Eck of the Kansas State Physics Department for their help with the Mossbauer Spectrometer. I would also like to thank Dr. Curnutte for designing and building the brass conversion electron detector. I also wish to thank Dr. Subash Kanetkar, a visiting professor in the Physics Department, for his assistance with the Mossbauer Spectrometer and for providing the plexiglass conversion electron detector. I also wish to thank Scott Griffin for the use of his computer in preparing this manuscript. I would also like to thank Jim Ed Wooldridge, a summer undergraduate research fellow, who synthesized one of the ligands used in this work. I would also like to thank Kansas State University and the Petroleum Research Fund for their financial support. Finally, I would like to thank Dr. Keith F. Purcell for his support and guidance during this project.

Table of Contents

LIST OF TABLES

LIST OF FIGURES

INTRODUCTION

Spin Crossover

Compounds containing d^4 through d^7 transition metals in an octahedral configuration may exist in the high spin or low spin electron configuration depending on the ligand field strength, Δ, relative to the spin pairing energy, P. In the case of weak field ligands, $\Delta < P$, the complex will exist in the high spin configuration. On the other hand, if $\Delta > P$, strong field ligands such as CN^- will result in a low spin configuration (see figure 1).[1] If the difference between these terms, $|\Delta - P|$, becomes small enough (on the order of kT) then both spin states may be populated and exist in thermal equilibrium, with the actual ratio depending on the temperature and pressure of the system. This phenomenon is referred to as spin crossover.

Characterization of spin Crossover

The spin crossover phenomenon is experimentally characterized by a plot of the high spin fraction (f_H) of a sample as a function of sample temperature (see figure 2). Two important features of such a plot are the temperature of the "discontinuity" in f_H vs T and the slope of the plot at this temperature. In real samples, this slope is finite, and the discontinuity is

Figure 1

Energy-level diagrams for d orbitals in octahedral iron(II) complexes ($3d^6$ electron configuration) for various relationships between Δ (splitting energy) and P (pairing energy).

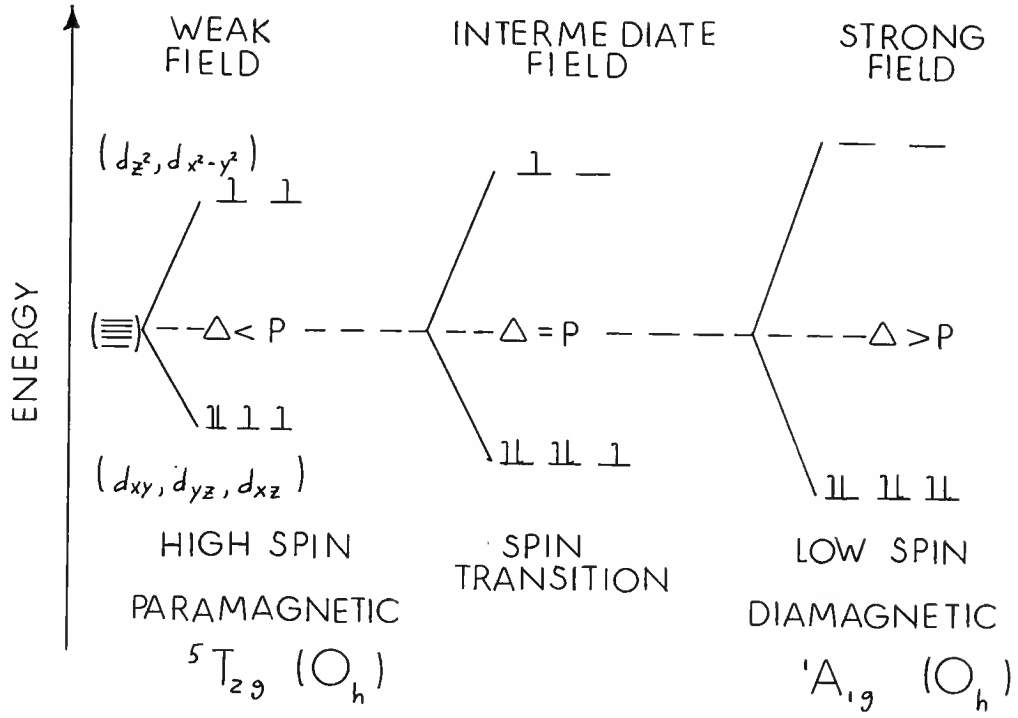
WEAK FIELD
INTERMEDIATE FIELD
STRONG FIELD
ENERGY
$(d_{z^2}, d_{x^2-y^2})$
(d_{xy}, d_{yz}, d_{xz})
$\Delta < P$
$\Delta = P$
$\Delta > P$
HIGH SPIN
PARAMAGNETIC
$^5T_{2g}$ (O_h)
SPIN TRANSITION
LOW SPIN
DIAMAGNETIC
$^1A_{1g}$ (O_h)

Figure 2

Temperature dependence of the high spin fraction, f_H.

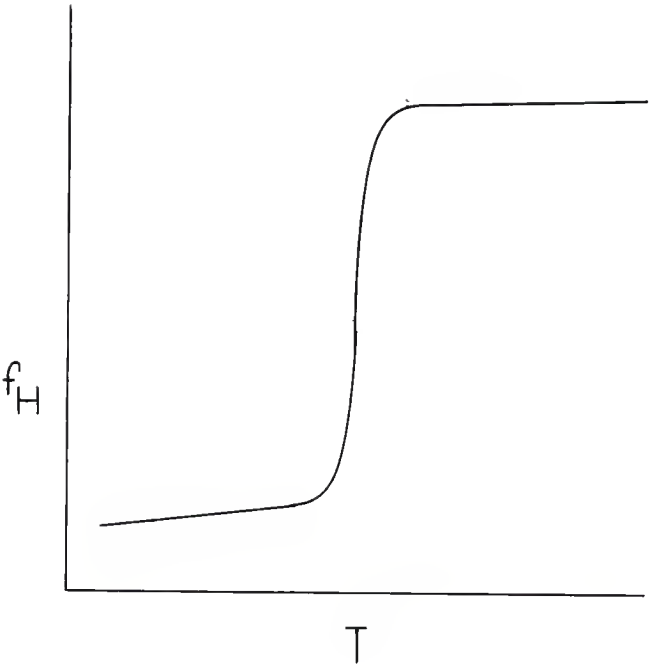
f_H
T

preceded, and followed, by regions of curvature. Also, the transition may be "incomplete" in that $f_H \neq 0$ at low T.

The driving force of a low to high spin conversion (with $\Delta H > 0$) is the change in entropy, as shown in the change in the Gibbs free energy for conversion of pure low spin to pure high spin phases:

$$\Delta G = G(HS) - G(LS) = \Delta H - T\Delta S \qquad (1)$$

from which one can define a transition temperature for the spin crossover as that at which there exist equal amounts of high and low spin molecules; in that case, $\Delta G = 0$ and[2]

$$T_c = H/S \qquad (2)$$

At absolute zero the $T\Delta S$ term vanishes and the change in free energy necessary to effect the change is equal to the change in enthalpy. Depending on the existing conditions (ie. ligands, pressure, etc.), if the temperature is low enough the enthalpy term will dominate. The importance of the ligands can be seen by comparing the compounds $[Fe(2\text{-pic})_3]Cl_2$[3] (2-pic = 2-aminomethylpyridine) and $[Fe(phen)_2(NCS)_2]$[4] (phen = 1,10-phenanthroline. The tris 2-pic complex undergoes

spin crossover at about 110 K, while the bis phen complex remains in the low spin state up to 230 K. Thus, replacement of three 2-pic ligands by two NCS^- and two phenanthroline ligands causes the enthalpy term to remain dominant until a higher temperature.

The ΔH and ΔS terms can be considered to be composed of various contributions:[5]

$$\Delta H = \Delta H_{el} + \Delta H_{intravib} + \Delta H_{latvib} \qquad (3)$$

$$\Delta S = \Delta S_{el} + \Delta S_{intravib} + \Delta S_{latvib} \qquad (4)$$

The 'el' subscript refers to the electronic contribution or change brought about by the spin change. The 'intravib' and 'latvib' subscripts denote, respectively, the intramolecular and lattice vibration contributions to the transition. The electronic contribution to the entropy is composed of contributions from spin and orbital degeneracies. However, since the spin transition compounds normally have less than cubic symmetry, the orbital contribution usually vanishes.

It has been shown by Sorai and Seki[6,7] that the most important entropy contribution comes from the vibrational changes brought about by the transition. The change in intramolecular metal-ligand stretching and deformation vibrations comprise two-thirds, and the

change in intermolecular lattice modes provide about one third, of the total entropy change. Nearly 50% of the intramolecular vibration change comes from the change in the metal-ligand stretching frequencies.

The spin conversion has been observed in both the solid and the liquid phases. The liquid phase has attracted only limited attention, but seems to be the best for isolating the effect of ligand substitution on the magnetic behavior; in solution the influence of intermolecular interactions between crossover molecules are omitted. The technique used in studying the spin crossover in solution is the Evans NMR method. Here, the change in the paramagnetic shift of solvent proton resonance positions is measured as the temperature is varied.[5, 8, 10]

Unlike the solution studies, where the behavior of discrete solvated molecules is observed, in solids the effect of the change in the lattice must be taken into consideration. There are several effects that must now be considered, such as lattice changes and intermolecular interaction, when the sample undergoes the phase transition. A phase is defined as an assembly of atoms or molecules that have attained equilibrium under specified external constraints and, in doing so, forms a distinct homogeneous region. The external constraints are usually taken as thermodynamic

properties such as volume, pressure, temperature. An isolated phase is stable only when its free energy is a minimum for the specified thermodynamic conditions.[11,12]

Upon undergoing spin conversion, the solid converts to a new phase, in this case a new magnetic phase. In a low spin to high spin transition, the change is accompanied by a corresponding change in the lattice structure. The transition generally results in an increase in the lattice size.[13,15,16] Gutlich et. al.,[17-19] using the $[Fe(2\text{-pic})_3]Cl_2 \cdot EtOH$ system, showed the change in the lattice size due to the spin transition (61 $Å^3$) is greater than that for the thermal expansion of the pure singlet phase over a typical two degree transition temperature change (0.8 $Å^3$). Furthermore, for this compound, Mikami et. al.[16] showed that while the lattice increased in size during the spin transition, the sample retained its original crystal structure in the new, high spin, phase.

A barrier that must be overcome for the phase change to occur is derived from the intermolecular interactions. The latter act to inhibit the phase transition by stabilizing the old phase through outer coordination sphere support. Here, neighboring molecules act to prevent the conversion to a new phase by mutual support. This concept is developed fully in a later section, as a progression from the

phenomenological level down to the molecular level is made in the description of the phase transition.

Solid State Concepts Important to Spin Crossover

Classically, a phase transition occurs in an ideal structure when the thermodynamic constraints that are placed on the system lead to a new minimum in free energy. Unlike an ideal system, in a real sample the equilibrium state is strongly affected by defects, such as vacant lattice sites, interstitial atoms, dislocations, stacking faults and grain boundries. Before proceeding, it is appropriate to define these solid state terms. Defects shall be defined as any natural or manufactured inhomogeniety within the crystal lattice. A stacking fault results when the regular crystal lattice stacking pattern is disrupted at one plane. This results in the formation of a new regular repeating sequence and a lowering of symmetry at that layer. An example is given below for an AB stacking sequence.[12]

ABABABBABABAB

The two neighboring B planes throw off the stacking sequence for one plane, then it continues on in a regular AB pattern. A "dislocation" is a line

discontinuity that separates two regions displaced by an interposing glide plane. Furthermore, the dislocation must either begin and end at the surface of the crystal or must form a closed line or part of a network in the interior of the crystal.[11] Grain boundries are formed when the crystals grow out of a solution. Crystals start growing at many points in the solution. When several of these growing crystals meet and form a lattice network the orientations of the individual crystal lattice surface planes may differ from one grain to another. These individual crystals are referred to as grains of the structure and the regions where the lattice orientation change occur are called grain boundries.[11]

The proposed mechanism for a solid state phase transition involves the nucleation and growth of the new phase around lattice defect sites such as those mentioned above. The transition can be analyzed using thermodynamics concepts. The thermodynamics used to describe the solid state phase transition can be analyzed from two different points of view, depending on one's perspective of "bulk" or "molecular" levels. The "bulk" view[11,12,20] utilizes macroscopic concepts to describe the over all transition, while the "molecular" view[2,21] focuses on the molecular origins and interactions during the growth of the new phase. As a result, the "bulk" view tends to combine terms that are

explicitely identified in the "molecular" view. A major difference between these two views is that the "bulk" view presumes long-range order in the new phase while the "molecular" view does not. The "bulk" view assumes homogeneous expansion of the new phase throughout the sample, whereas the "molecular" view makes an allowance for this and for intermingling of the two spin phases during the growth of the new phase.

Bulk and Molecular Interpretations

The "bulk" expression for the free energy of a sample as the new phase develops within the original phase is given as[11]

$$\Delta G = n(g(hs) - g(ls) + \Delta g_s) + \Delta g_{sa} \qquad (5)$$

Where the quantity g(hs) - g(ls) is the change in free energy between the two pure phases and Δg_s is the change in free energy due to strain (deformations or dislocations) induced in the host and new lattices as the new phase develops. This term is also known as the strain energy. The Δg_{sa} term is a surface free energy term depending on the size and shape of the expanding phase. n in equation (5) is the number of molecules in the forming region.

A phenomenological approach (Slichter and Drickamer)[21] which can be adapted to a "molecular" view of the

transition is derived from the expression

$$-\Delta G' - \Gamma(1-2f_H) = RT\ln K = -\Delta G \qquad (6)$$

The quantity K is calculated as f_H/f_L (where f_L is the fraction of low-spin species). Γ is a nonlinear Gibbs energy parameter and the factor $(1-2f_H)$ renders (6) transcendental in f_H; f_H is the fraction of quintet spin molecules in the sample. The free energy of the system, G, at any point during the crossover can be expanded as follows (Purcell and Edwards).[2]

$$G = G_{free} + G_{mix} + G_{inter} \qquad (7)$$

The term G_{free} is the Gibbs free energy associated with isolated molecular behavior ($G_{free}=G_{el}+G_{intravib}$ see (3) and (4)); G_{mix} is the energy derived from maximization of ensemble probability and G_{inter} reflects the effects associated with cooperativity, lattice continuity and domain formation.

From developing G as a function of f_H and λ (the length of a physically continuous region) one arrives at

$$\Delta G' = \Delta G_{free} + (1-1/\lambda)(G_{HH}-G_{LL}) \qquad (8)$$

and

$$\Gamma = (G_{HL}-G_{LL}) + (G_{HL}-G_{HH}) \qquad (9)$$

where G_{ij} is the Gibbs energy of interaction between molecules of spin types i and j, H and L. λ is determined by the number and types of lattice defects. Comparing equation (6) with equation (5) and using equation (7) reveals the following associations:

$$n(g(hs)-g(ls)) \longleftrightarrow \Delta G_{free} + (G_{HH}-G_{LL}) = \Delta G' + \tfrac{1}{2}(G_{HH}-G_{LL}) \qquad (10)$$

and

$$n\Delta g_s + \Delta g_{sa} \longleftrightarrow -\tfrac{1}{2}(G_{HH}-G_{LL}) + (1-2f_H)\Gamma \qquad (11)$$

With this in mind, let us first consider the implications of the "bulk" thermodynamics of the phase transition at temperatures along the transition process and the role of lattice defects in the transition.

To achieve more than 50% conversion of the low spin phase to the high spin phase, the $T\Delta S$ term must be larger than the ΔH term when both terms are positive, as seen in equation (1), since the free energy change ΔG must become negative. In the bulk formalism, since Δg_s and Δg_{sa} are positive quantities as the transition temperature is reached, it is necessary that

$$g(hs) - g(ls) < 0 \qquad (12)$$

While this condition is required, additional corrections which represent a barrier to the transition are also present. This barrier is due in part to the Δg_s term in equation (5). As the new phase begins to grow, the volume change in the new lattice distorts the surrounding host lattice such that an appreciable energy barrier to conversion may develop. The transition will occur along the lowest free energy pathway. In order for this to happen, Δg_s must be minimized. This means that as few molecules as possible in the host lattice must be dislocated. Sites that minimize Δg_s in this manner are referred to as preferred sites. These preferred sites tend to occur at defect sites where there exists an inhomogeniety in the lattice, rather than at sites of nearly perfect lattice.[//] This inhomogeniety allows the new lattice to form with less energy needed to displace the surrounding lattice. This lowering in the energy is greatest at extended defects, such as the intersection of grain boundries, which form the edges and corners of the grains.[//] Another location at which the barrier is lowered is at the surface of the crystal, at which an average of 50% of each molecule lacks first and subsequent coordination spheres.

The importance of these extended defect sites is due to the ability of these sites to accomodate the lattice shape and volume changes at much lower temperatures than do regions of nearly perfect lattice. This tends to reduce the strain energy term to nearly zero, which then results in a lower free energy of nucleation and coresponding increase in the nucleation probability.[11]

Now that the sites of nucleation of the new phase have been identified we can now consider the growth of the new phase in a crystal lattice. The transition is considered to begin when a small, homogeneous region of the new spin phase forms and begins to spread outward. As the region spreads out, the final free energy term , Δg_{sa} from equation (5), gains and then loses importance as the 50% conversion point is approached and passed. This term is a reflection of both the size and shape of the expanding region. That is, certain shapes are more easily spread through a lattice than others. According to the "bulk" view, the easist shape for region expansion approximates a two dimensional disk (oblate spheriod).[11,12] One dimensional "regions" are "generally" not considered, due to the probability of growth in only one direction being far below that for expansion across a surface. In the "bulk" view, the expanding region is considered to expand in both directions at the same time, if possible. However,

although one might be inclined to believe that a three dimensional phase region will be more favorable for propagation, a disk shaped area will displace less of the host lattice and thus require less energy for conversion. The greater the surface area of the expanding region, the larger the correction factor must be. The surface area is determined by the region shape, as different shaped regions have different surface areas, and by the region size, or the number of atoms in the region. The more atoms present, the larger the size of the region, which increases the surface area. Thus, the surface energy term increases as the region grows and acts to increase the change in the free energy needed to propagate the transition.

As the new phase continues to grow, it may encounter structural barriers to propagation. These will take the form of other defects. As the phase propagates through the lattice and encounters a defect, the energy to continue the expansion in that direction increases.[12] The lattice sites initially beneficial for nucleation have now become a hinderance to continued region expansion. Extended defects such as lattice dislocations and grain boundries will tend to stop the expansion. Small defects, also referred to as point defects, such as Schotky or Frenkle defects or foreign atoms, will act as local barriers to expansion. With

the point defects, the only portion of the expanding region stopped or hindered is that region which meets the defect, all the other areas may continue to grow normally. When the expanding region meets an extended defect, growth in that direction is halted in preferrence to the already propagating directions of lower activation energy. As a result, growth across a grain boundry or lattice dislocation will tend not to occur until the entire crystal grain or region is converted to the new spin phase.

We have now reached the final feature of interpretation of equations (5) and (7). It remains to identify in $n\Delta g_s + \Delta g_{sa}$, or Γ, the role of cooperativity in the transition. Cooperativity is defined as the inhibitive effects of the coordination spheres surrounding each molecule on the nucleation and proagation of the new phase. This contribution to ΔG, and therefore to the propagation barrier, increases with the number of homogeneous molecular contacts acting to retain a molecule in its initial spin state. Thus, both Δg_s and Δgsa implicitly arise from the Gibbs energies of interaction between like-spin and different-spin molecules. The definition of Γ, equation (9),[2] explicitly identifies the origin of cooperativity in such interaction energies as due to less stable H-L than H-H or L-L interactions. Defects present sites of

minimum energy to initiate the transition. Here, inhomogeniety in the surrounding coordination spheres lowers the intermolecular coupling energies G_{ij} and this results in a minimization of $\Delta g_s + \Delta g_{sa}$, or Γ at those sites. From Purcell and Edwards

$$T_c = \Delta H/\Delta S \qquad (2')$$

and

$$\text{slope}\{f_H \text{ vs } T\} \text{ at } T_c = \Delta H/RT_c^2[1-\Gamma/2RT_c] \qquad (13)$$

where

$$\Delta H = \Delta H_{free} + (1-1/\lambda)(H_{HH}-H_{LL}) \qquad (14)$$

$$\Delta S = \Delta S_{free} + (1-1/\lambda)(S_{HH}-S_{LL}) \qquad (15)$$

Thus, the defect sites can be seen as being very important to the nucleation and growth of the new phase by virtue of the affects of such defects on λ and on Γ.

For the new phase region to persist in the lattice, the phase must attain a critical size dependent upon the size of the region or grain it is propagating in. If that is not possible, due to insufficient thermal energy, then the new phase region will revert back to

the old phase. The probability of reversion decreases as the new phase grows, due in part to the molecules of the new phase providing mutual support through intermolecular interaction. Thus, while the cooperativity phenomenon originally hinders propagation of the new phase, once the new phase forms the cooperativity acts to stabilize and maintain it.

Two chemical factors that affect the spin transition in a fashion analogous to that of physical defects are metal dilution[5,15,22-25] [decreasing x in $(Fe_xM_{1-x})L_n$] and the anion[3,5,26] (if any) that is present. The shift in the transition temperature due to the anion is directly related to the lattice structure. Generally, the anion will act as a bridge (through electrostatic or hydrogen bonding attraction) between spin crossover cations. This allows the anion to actively participate in communicating the spin state changes from one molecule to another. The change in the vibrational and lattice elastic properties with dilution or anion will dictate how effective the cooperativity will be. Regarding metal dilution, as the fraction, χ, of iron in the compound decreases, intermolecular contacts between Fe chelates diminishes and the transition moves to lower temperatures and becomes more gradual (less cooperative).

Experimental Support for the Importance of Lattice Defects on Spin Crossover

Two experiments that show the effect of defects in the crystals were conducted by Casey et. al.[27,28] (also see Baker and Bobonich[29]) and Hendrickson et. al.[30,31] Casey's work centered around the effect of crystal preparation on the transition. He showed that slow Soxhelet extraction of $[Fe(phen)_3](NCS)_2$ to give $[Fe(phen)_2(NCS)_2]$ produced well formed crystals that (1) had no high spin fraction at low temperatures and (2) underwent a sharp phase transition. On the other hand, a rapid extraction produced small, poor quality crystals that contained a considerable high spin fraction at low temperatures, with a transition that is still somewhat sharp. Fast extraction results in small crystals that contain more defects than the slowly formed sample. A considerable number of the defects in the poor quality material will be major defects such as grain boundries and lattice dislocations. The increase in the number of grain boundries is due to the formation of many small grains rather than larger crystal grains. Likewise, the rapid extraction will result in a greater number of various types of dislocations and faults in the lattice than if the crystals had been allowed to grow slowly. These smaller phase regions of small grains or single grains divided into many separate regions due to faults

and dislocations will result in less of a change in the free energy to reach the critical size. Thus, the over all energy needed to totally convert this region into the new phase is smaller than for large crystal regions and grains. This means that the phase transformation can occur at a lower temperature. Also, as a result, several small regions of the high spin phase can form in the poorly crystallized material and persist without reverting to the low spin phase at low temperatures. The well formed crystals consist mainly of larger grains relatively free of major defects and as a result, require higher temperatures to bring about a conversion to a different spin phase.

Recall that major defects such as grain boundries tend to discourage the expansion of a spin phase region. Thus, just as the major defects inhibit the expansion of the spin-converted region they also inhibit its return to the previous spin phase. As a result, once a region, set off by major defects, is converted to the new spin phase it is held in check from reverting to the initial phase by the activation barrier that also protects it from the surrounding grains of the old spin phase. Therefore, a fraction of the high spin phase is expected to exist in the sample after the bulk transition temperature is passed upon cooling.

Hendrickson's work[30,31] reached similar conclusions,

in that it showed that grinding a sample of $[Fe(3\text{-}OCH_3\text{-}SalEen)_2]PF_6$ (SalEen = the monoanion of the condensation of salicylaldehyde and N-ethylethylenediamine) causes a high spin fraction to develop at low temperatures and to persist upon cooling. Furthermore, the grinding decreases the sharpness and completeness of the transition. In this case, instead of many small grains and dislocations forming during crystallization, Hendrickson used well formed crystals and ground them to introduce dislocations, faults and fractures in his crystals. The greater the period and severity of grinding, the greater the number of defects.

As several sections of the grain convert to the new spin phase, a region of the old spin-phase may become trapped within the surrounding new spin-phase region. As the transition temperature is reached and passed, the energy to convert the old spin-phase region may be reached; however, because the old phase is trapped within the new spin phase lattice an old problem rearises. This problem is the dislocation energy. Now that the low spin region is surrounded by the high spin region it cannot be as easily converted to high spin because it may lack the energy needed to expand its lattice outward and displace the high spin lattice. The result of this is that the Δg_s term in equation (5) is now very large. This favors the retention of the low

spin phase in the trapped region. This is not seen in the unground samples due to the fact that most of the grains are not heavily fractured into small nearly independant regions and the grains tend to undergo the transition all at once.

Conversion Electron Mossbauer Spectroscopic Probe of Spin Crossover

As stated previously, the spin phase transition tends to initiate at major defect sites due to a lower change in the free energy for these sites. Three possibilities exist as to the location of where the transition begins. The transition may begin at interior defect sites, at surface sites or at regular lattice sites. The subject of this research is to experimentally determine whether the transition begins at surface sites and then works inward.

To test this hypothesis, Conversion Electron Mossbauer Spectroscopy (CEMS)[32] results will be compared with the results obtained from Transmission Mossbauer Spectroscopy.[33] The transmission technique is a bulk sampling technique, in that any ^{57}Fe nucleus in the sample can absorb the γ-photon emitted from the source. This will show up as a transmission dip in the final spectrum. Using this technique, the observed spectrum is dominated by absorption from the regular lattice

atoms.

CEMS, however, is a surface sensitive technique in which an ^{57}Fe ejected K-shell electron is the entity detected, instead of attenuation of the incident γ-photon beam. What makes this technique surface sensitive is that the electron has a finite escape depth, such that below a certain depth within the sample the ejected electrons cannot reach the surface with energy sufficient to escape and register the absorption event. The escape depth of the 7.3 keV conversion electron is the depth from the surface that produces 66% (1/e) of the total number of detected electrons. This depth is quoted most often[34] as 54 nm (540 Å). Roughly 95% of the detected electrons come from a distance of about 300 nm (3000 Å). Employing energy analysis of the conversion electrons will allow depth profiling of the sample, higher energy electrons coming from nearer the surface.

Now that we know what will be detected and where that entity originates in the sample, it seems prudent to discuss how this entity, the 7.3 keV electron, is generated. When a ^{57}Co nucleus in the source decays to an initial excited ^{57}Fe nuclear level, it passes through a number of lower excited states. Eventually, nearly all nuclei reach the first excited state, 14.4 keV. Ten percent of the nuclei in this state relax to the ground

Figure 3

Energy-level diagram of the ^{57}Fe nucleus, showing photo excitation to the first excited state and subsequent relaxation pathways.

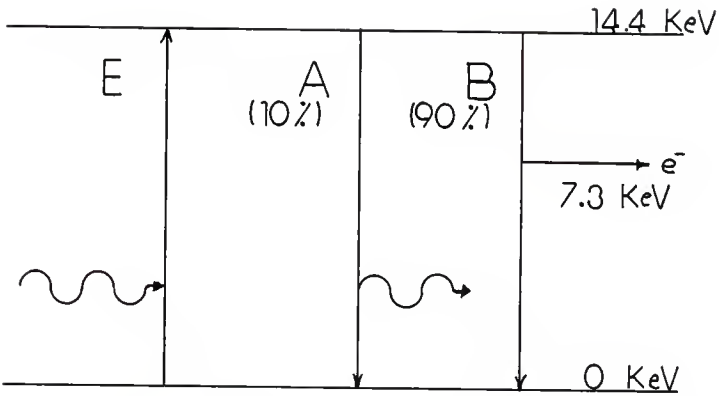
14.4 KeV
E
A
(10%)
B
(90%)
e⁻
7.3 KeV
0 KeV

state by emitting a 14.4 keV photon. Upon striking an ^{57}Fe nucleus in the absorber the γ-photon is absorbed if there is an energy match between the photon and the absorber nuclear level energy gap (see figure 3). If the γ-photon is absorbed, then the absorber ^{57}Fe nucleus is promoted to its first excited state, E in figure 3. Since the excited state is unstable, the nucleus will relax back to the ground state, just as the source nucleus did. To do this, the nucleus must release energy. Again, 1 out of 10 of the excited nuclei will re-emit the γ-photon with the same energy (transition A in figure 3). The preferred relaxation process (B, about 90% efficient) is to eject a K-shell electron with an energy of 7.3 keV. These electrons are often referred to as internal conversion electrons.

When a conversion electron is ejected from an ^{57}Fe atom near the sample surface into the detector gas it causes the formation of a number of electrons (n) in proportion to its energy.

$$nD + e^-_k \longrightarrow nD^+ + (n+1)e^- \qquad (16)$$

These electrons are drawn toward the anode wire and register as a surge in the detector current. The magnitude of the surge is determined by the energy of the conversion electron. Later chapters will include

information and schematics of the detectors actually used in this work and the difficulties experienced with them.

At least three different proportional detector designs have been reported.[30-43] They all employ the same basic concepts, but they differ in their assembly. Other types of detectors include parallel plate avalanche counters, Auger electron spectrometers with electrostatic cylindrical mirror analysers and channel electron multiplier based systems.[35]

The detector consists of a sealed body with windows on opposite body faces. These windows are generally 3 to 5 mil thick ^{57}Fe-free aluminum foil or Mylar. An anode wire runs from a high voltage connection at one end of the detector to the other end and back. This is a continuous, closed circuit that will be used to detect a current surge, to be discussed later. The final feature required is a gas inlet and an outlet. Unlike the transmission detector which is a static, or closed, system, the CEMS detector employs a dynamic flowing gas detector, which requires gas inlet and outlet parts. A variety of materials such as brass, aluminum and plexiglass can be used in the fabrication of the body. Hollow cylinder and hollow rectangular box shapes have been reported in the literature for the detector.

Another major difference between the CEMS and the

transmission experiments is that in CEMS the sample must be mounted inside the detector. This is necessary so that the ejected electron will pass directly into the detector gas without losing a substantial amount of energy. Sample mounting on either window is acceptable; however, most researchers prefer to have the sample on the back window. This technique is referred to back scatter CEMS. In all actuality, there should be no observable difference in the spectra produced by the two sample mounts.

The choice of detector gas is critical. It is desired to detect only the low energy electrons while ignoring the incident 14.4 keV photons, 6.3 keV X-rays and other high energy photons.[34] These latter entities generate an undesirable backround noise. To reduce the detection of these photons a detector gas that has a poor efficiency for the absorption of these unwanted entities should be used. The type of gas most often used in detectors such as these is a noble gas, although good results can be obtained using N_2. Of the noble gases, that with the lowest efficiency for capture of photons is helium. A quencher gas is also required to prevent the ionization of helium atoms by photons resulting from the recombination of an electron and the helium ion. The quench gas is able to absorb the photon without becoming ionized and then release its excess

energy through a combination of thermal and photon emission relaxation processes such that helium nuclei will not be ionized.[44] Methane is generally used; however, other lightweight hydrocarbons may also be used, as may ethanol.

To achieve energy analysis of the electrons[35] (pulse height proportional to electron energy), it is necessary to have the gas thickness greater than one third of the Bethe range (the zig-zag collision distance of the electron in the gas). For the 7.3 keV electrons this range is about 8.5 mm. Thus, the thickness of the gas should be at least 3mm. Various groups have used thicknesses ranging from 2 to 10 mm.[35] Values smaller than the recommended thickness will still produce meaningful results, although they will suffer from incomplete energy resolution and a slight deviation from electron-count/electron energy proportionality. This will result in truncation of the exponential energy dispersion of conversion electron energies, as the highest energy electrons (those from the surface) will not be completely stopped by the gas inside the detector.

The goal of this work is to attempt to observe a difference in f_H/f_L as determined by the spectra taken by CEMS and by transmission spectroscopy. This will then be used to determine whether the spin transition

starts at the surface of the crystals or at bulk or interior sites. Based on the ideas of the previous section, the transition should start at the surface and spread inward. If this is true, a corresponding shift in the temperature of the transition should be detected, such that f_H / f_L at $T < T_c$ will be greater for CEMS than for transmission spectra.

Selection of materials for this study is limited by the detector design, since low temperature spectra can not now be obtained. Thus, compounds that undergo a spin transition at or around room temperature were needed. The first compound chosen was $[Fe(2\text{-pic})_3]Cl_2 \cdot H_2O$, prepared by Gutlich et. al.[45] After several attempts to synthesize this compound failed, it was decided to work with other compounds.

The new compounds have the formula [Fe(X)L], where L = 4-azaheptamethylene-1,7-bis(salicylideneiminate) (see I) and X = pyridine or methyl substituted pyridine (see II). These compounds were originally prepared by Matsumoto et. al.[46] In order to extend the series of materials to examine, and to probe the effect of changing the subtituents on the pyridine, additional, new complexes were prepared in which the methyl groups on the pyridine ligand of Matsumoto's complexes were oxidized to carboxylic groups.[47] This ligand modification should lower the transition temperature due

L =

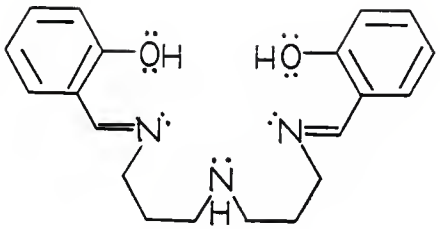

I

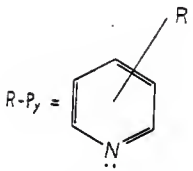

II

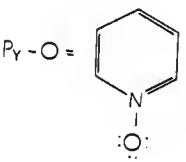

III

to a withdrawl of electrons from the ring and, thus, a reduction of the σ donor character of the pyridine nitrogen. The pyridine-N-oxide complex was also prepared (see III), as it is expected that this compound would also undergo a spin transition at a lower temperature, due to the lower σ donor abilty of oxygen than nitrogen in pyridine. Finally, it was decided to examine the anion effects. The anion used in Matsumoto's work was BPh_4^-.[46] Materials were thus prepared with PF_6^- as the anion. This could result in a shift to a higher transition temperature since PF_6^-, because of its smaller size, could be less tightly associated with the cations and thereby reduce the size of the term $(H_{HH}-H_{LL})$ in (14).

EXPERIMENTAL

PREPARATION OF COMPOUNDS

Two different types of compounds were prepared in this work. The first type, the Fe(II) complex, $[Fe(2\text{-pic})_3]Cl_2\ H_2O$, was originally prepared by Gutlich et. al.[45,48] The second type of compound, a series of Fe(III) complexes, was originally prepared by Matsumoto et. al.[46] These compounds have the formula $[Fe(X)L]^{+n}$ (n=0 or 1) where L = 4-azaheptamethylene-1,7-bis(salicylideniminate) (see I) and X= Cl^- or a substituted pyridine molecule. In the case where X is not an anion (n=1), a counterion is present. The counterion is Cl^-, BPh_4^- or PF_6^-.

$FeCl_2 \cdot 2H_2O$. The first step in the synthesis of this compound was the preparation of Fe(III)-free $FeCl_2 \cdot 2H_2O$, as per Gayer and Woontner.[49] To obtain this, $FeCl_2 \cdot 4H_2O$ (24.0 g, 0.121 moles; Aldrich, 99+%) was combined with electrolytic iron (0.8-1.0 g, 0.02 moles; Fisher, purified), 38% HCl (1 ml) and distilled water (6.5 ml) and was placed in flask A (see IV).

The mixture in flask A was heated at 80° C to disolve the salt, then heated for 30 min more to completly reduce any Iron(III) present. The apparatus

was then inverted and the unreacted iron was separated

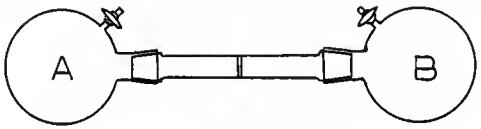

IV

by filtration through the frit. The light green solution in flask B was allowed to cool to room temperature, during which time light green monoclinic crystals were formed. The solution was allowed to sit for up to five hours after the solution reached room temperature to ensure complete crystallization. The apparatus was then inverted and the crystals were collected on the frit. The crystals were then dehydrated under nitrogen at 80 $^{\circ}$ C until they were light greenish-white in color. This was the desired dihydrate, isolated in 9.93% yield.

$[Fe(2\text{-pic})_3]Cl_2 \cdot H_2O$. To $Fe(II)Cl_2 \cdot 2H_2O$ (1.0 g, 7.86×10^{-6} moles), in just enough of a hot, deoxygenated 1:1 solution of ethanol and distilled water to disolve the complex, was added 2-picoline (2.50 ml, 7.95×10^{-6} moles; Aldrich, 99%) disolved in 15.0 ml of deoxygenated ethanol. The resulting solution was dark red-brown color. The hot solution was left to cool to room temperature and then left undisturbed for several days

to ensure crystallization occured. The solution was then placed in an ice bath for an additional two days to complete the crystallization. From this an undetermined, but poor, yield of rectangular, red-brown crystals (2-3 mm on a side) was obtained.

The remainder of the synthesis was not successfully completed, but is presented in order to document my results. The red-brown crystals above were recrystallized in a deoxygenated solution of a 10:90 mixture of distilled water to ethanol. This is reported to give pure crystals of $[Fe(2\text{-pic})_3]Cl_2 \cdot 2H_2O$, while the product actually obtained was a black tarry solid. To obtain the monohydrate, it is reported that the dihydrate can be heated at or above 75° C under nitrogen.

H_2L. This compound was prepared by mixing salicylaldehyde (0.2 mol, 24.424 g; Aldrich, 98%) and di(3-aminopropyl)amine (0.1 mol, 13.122 g; Aldrich, 98%) in 100 ml of methanol. This produces a yellow colored solution in an exothermic reaction. The desired product is a very viscous, dark yellow oil and is obtained by removing the methanol under vacuum. CARE SHOULD BE USED IN HANDLING OF THE AMINE REACTANT AND THE PRODUCT SINCE THEY ARE BOTH FAIRLY TOXIC.

[Fe(Cl)L]. This compound is the precursor for all the other Fe(III) compounds prepared. It was synthesized by adding anhydrous iron (III) chloride (10 mmol, 1.6222 g; Fisher, purified) in 50 ml of methanol to a solution of H_2L (10 mmol, 3.39 g) in 50 ml of methanol. This reaction was carried out in a glove bag under dry nitrogen atmosphere to prevent the hydration of the iron (III) chloride. (It should be noted that dissolving the iron (III) chloride in the methanol produced a yellow-brown solution in an exothermic reaction that also produced a small amount of white vapor (most likely HCl). The solution was stirred at 40 °C until the H_2L was completely dissolved. Upon mixing the two compounds, a dark wine colored solution was produced. This solution was stirred at 50 °C for 10 min and then triethylamine (20 mmol, 2.80 ml; Fisher, reagent) was syringed into the reaction vessel and the solution was stirred at 50 °C for 1 hour. During this time dark red-purple cyrstals form. The solution was left to cool to room temperature overnight and then filtered. The black solid recovered was washed with 15-20 ml of methanol, then 15-20 ml of diethyl-ether and dried in vacuo. The yield is 94%. The melting point of these air stable crystals is > 300° C.

[Fe(py)L]BPh_4. Pyridine (3 mmol, 0.237 g; Aldrich,

99+%, GOLD LABEL) was added to a dark red solution of [Fe(Cl)L] (2 mmol, 0.857 g) in 50 ml methanol. The reaction mixture was stirred at 60°C for 30 min, then filtered hot. To the filtrate was added a solution of sodium tetraphenylborate (0.2 mmol, 0.684 g; Fisher, certified) in 10 ml methanol. At this time small red crystals could be seen forming on the sides of the flask. The mixture was stirred at 60 °C for 5 min and was then allowed to slowly cool down to room temperature overnight. The black solid was collected and washed with methanol and diethyl ether and dried in vacuo. The yield was 90%. The black solid was made up of small red-brown rhomboid shaped crystals. These crystals decomposed at 162-4 °C.

[Fe(3Me-py)L]BPh_4. This compound was prepared using the same procedures as were used to prepare [Fe(py)L]BPh_4. Here, 3-picoline (3 mmol, 0.2794 g; Aldrich, 99.5+%, GOLD LABEL) was added to the precursor solution. As in the previous case, a black solid was recovered when the solution was filtered. The yield was 88%. The individual crystals appeared as dark red rectangular parallelepipeds that decomposed at 157-9 °C.

[Fe(3,4Me_2-py)L]BPh_4. This compound was prepared using the same procedures as were used to prepare the

previous compounds. Here, 3,4-lutidine (3 mmol, 0.3215 g; Aldrich, 98%) was added to the precursor solution. The resulting black precipitate was filtered, washed and dried, resulting in a 91% yield. The individual crystals appeared as dark red rectangular parallelepipeds that decomposed at 167-70 °C.

$[Fe(O\text{-}py)L]BPh_4$. This compound was prepared as above. Pyridine-N-oxide (3 mmol, 0.2853 g; Pfaltz & Bauer) was added to the precursor solution. The reddish-purple solid obtained upon filtration was washed and dried, giving a yield of 72%. The sample was composed of red rhomboid crystals that decomposed at 175-7 °C.

$[Fe(py)L]PF_6$. This compound could not be prepared as are the BPh_4^- salts, due to the insolubility of the KPF_6 in methanol. To prepare this compound, pyridine (3 mmol, 0.237 g) was added to a solution consisting of [Fe(Cl)L] (2 mmol, 0.857 g) in 50 ml of a 1:1 solution of distilled water and methanol. The resulting dark orange-red solution was stirred at 60 °C for 30 min, then filtered. To the filtrate was added KPF_6 (2 mmol, 0.3821 g; Aldrich, 98%) in 10 ml of the water-metanol solution. The resulting solution was stirred at 60 °C for 5 min, then allowed to return to room temperature

overnight. As the solution cooled, a reddish solid could be seen forming on the sides of the flask. The product was recovered as a dark red solid upon filtration and in a 57% yield, after being washed and dried in vacuo. No individual crystal form could be discerned for this sample that decomposed at 192-4°C.

Nicotinic acid (NA). This compound was prepared by Jim Ed Wooldridge (1986 Summer PRF Fellow) using the procedure set forth by Black et. al.[47] Since only a small quantity of the acid was required, the literature preparation was scaled down as follows. 3-picoline (10 g) was added to distilled water (125 ml) in a 3 neck flask. One neck contained a thermometer immersed into the solution, the middle neck contained a water-cooled reflux column and the third neck was stoppered. To this solution was added $KMnO_4$ (45 g) in ten portions over a period of six hours. The temperature of the mixture should start at 70 °C and be slowly increased to 90°C. Each $KMnO_4$ portion should be added to the solution only after the previous portion has been consumed (a purple to brown color change). The $KMnO_4$ should be washed down the walls of the column with distilled water, using as little as possible, so as not exceed a total of 25 ml.

After the last portion is consumed, the hot solution was suction filtered to remove the MnO_2 from the

solution. The MnO_2 was then washed four times with distilled water (75 ml each). The cake was allowed to thoroughly dry before each wash and suction was not applied until the water had a chance to soak into the cake.

The filtrate was then evaporated down to 150 ml and the pH set to about 3 by the addition of 13 ml HCl. The solution was heated to 95-100 °C to dissolve any precipitate and then allowed to slowly cool to room temperature. WARNING: Rapid cooling causes the crystals to be contaminated with KCl. The solution was then cooled for several hours in an ice bath. The precipitate was then filtered out and washed with 5 ml of cold water.

Further crops were extracted by reducing the volume of the solution, heating the solution to 95 °C and then allowing the solution to slowly cool.

3,4-Dipicolinic acid (DPA). This compound was prepared using the procedure set forth for the 2,6-dipicolinic acid as set forth by Black et. al.[47] Again, due to the small amount of this product required in the complex syntheses, the procedure was scaled down as follows. 3,4-lutidine (5.35 g, 0.05 mol) was added to distilled water (125 g) in a 3 neck flask. The flask was arranged as in the previous preparation. Over 17

hours, $KMnO_4$ (41.9 g, 0.265 mol) was added to the solution in ten portions. The temperature of the mixture should start at 70°C and be slowly increased to about 95°C. Again, each portion was completely consumed before the next was added. A total of 75 ml of water was used to wash the $KMnO_4$ down the sides of the column.

After the last portion was consumed, the solution was filtered hot to remove the MnO_2. The cake was washed with four portions of water (75 ml each), as above.

The filtrate was evaporated down to 100 ml and acidified to a normality of about 1.5 by the addition of 25 ml conc. HCl. The solution was heated to boiling to dissolve any solid and allowed to slowly cool to room temperature (see the warning above concerning rapid cooling). Following this the solution was held at 5 °C overnight (7-8 hours). The white crystals were filtered off and washed with 10-15 ml of water and left to air dry.

A second crop of crystals were obtained by concentrating the filtrate to 60 ml and then cooling at 5°C for 7-8 hours. The reaction produced an 84% yield.

[Fe(NA)L]Cl and $[Fe(NA)L]BPh_4$. The sytheses were conducted using the same procedures set forth for $[Fe(py)L]BPh_4$. Here, nicotinic acid (3 mmol, 0.3693 g)

was added to the precursor solution and was stirred at 60 °C for 30 min. The solution was then filtered hot, yielding a dark purple solid (0.27 g) in 25% yield with no discernable crystal structure and a melting point greater than 300 °C. The solid product recovered at this point in the synthesis was the Cl^- salt.

To the filtrate was added sodium tetraphenylborate (2 mmol, 0.684 g) in 10 ml methanol. The solution was stirred at 60 °C for 5 min, then left to return slowly to room temperature overnight. Filtration yielded a light purple solid (0.43 g) in 26% yield with no discernable crystal form and that decomposed at 214°C.

[Fe(3,4-DPA)L]Cl and [Fe(3,4-DPA)L]BPh_4.
3,4-dipicolinic acid (3 mmol, 0.501 g) was added to the precursor solution and was stirred at 60 °C for 30 min. The solution was then filtered hot to yield a dark purple solid (0.28 g) in 24% yield with no discernable crystal form and a melting point greater than 300 °C. Again, the product recovered at this point in the synthesis was the Cl^- salt.

To the filtrate was added sodium tetraphenylborate (2 mmol, 0.684 g) in 10 ml methanol. The solution was stirred at 60 °C for 5 min, then left to slowly return to room temperature overnight. Filtration yielded a reddish-purple solid (0.77 g) in 44% yield with an

octahedral prism crystal form. The compound decomposed at 228-9 °C.

INSTRUMENTAL METHODS

Electron spin resonance spectra of polycrystalline samples were collected at room temperature on a Bruker Model ER 200D-SRC using an X-band microwave bridge and a rectangular cavity. A suitable solvent could not be found to do solution phase studies.

Infrared spectra were obtained as nujol, carbon tetrachloride and chlorofrom mulls on potassium bromide plates. The spectra were collected on a Perkin-Elmer 1330 Infrared Spectrometer. Polystyrene was used as a wave number calibrant.

Magnetic susceptibility measurements were obtained at room temperature using a Cahn/Ventron Faraday Magnetic Susceptibility System model #7600. The effective magnetic moments were calculated from $\mu_{eff} = 2.83(T\chi)^{1/2}$. $HgCo(SCN)_4$ was used as a calibrant and the susceptibility of [Fe(Cl)L] was used as a check on the calibration. [Fe(Cl)L][46] is a high spin complex with a constant μ_{eff} (5.82) over a large temperature range, 85-300 K. Diamagnetic corrections were made using values given by Mulay and Boudreaux.[50]

Melting points were taken using a Fischer-Johns Melting Point Apparatus from Fischer Scientific

Corporation.

Mossbauer spectra were obtained using a locally constructed system to be described in the next section. The source used was 25 mCi ^{57}Co in a palladium matrix from Isotope Products. The Doppler velocity scale was calibrated with an enriched ^{57}Fe foil absorber. This calibration was used for both the transmission and the conversion electron spectra. Crystalline samples were sealed between two sheets of Parafilm or packed into a plastic tube, sealed at one end by 3M tape, for the transmission spectra. For the brass conversion electron detector, the sample was mounted on a piece of ^{57}Fe-free aluminum foil using Duco cement and the aluminum foil was grounded with conductive silver paint. The same arrangement was used with the plexiglass detector except that the sample was physically grounded by a wire rather than with conductive paint.

^{1}H nuclear magnetic resonance and mass spectroscopy were both attempted without success.

MOSSBAUER SPECTROMETER SYSTEM

Drive Unit:

The Doppler drive unit consists of a ferromagnetic iron rod which is rigidly supported at both ends by flat, circular, metal springs and passes through a

magnetic pick up coil. Output from this coil allows one to monitor the quality of the mechanical motion with an oscilloscope. The rod was driven in the constant acceleration mode by a double coil accoustical speaker, to which one of the springs was rigidly attached by a short section of threaded steel rod. ^{57}Co in a palladium matrix source was mounted, via a threaded rod, to the other spring.

The velocity at which the speaker drives the source was set by a locally built signal converter acting on a sawtooth wave generated by a 3311A Hewlett-Packard frequency generator. A feedback wire running from the second speaker coil to the signal converter allows the driving signal to be corrected for discrepancies in the mechanical response to the sawtooth driving wave. The correction was superposed on the driving signal sent to the primary speaker coil.

Detector system:

Three different detectors were used in this work. For transmission measurements, a commercial argon/ methane photon detector was used due to its efficiency in detecting γ-rays. The other two detectors were both locally constructed conversion electron detectors. The first of the two detectors (see Figures 4-11) was designed by Dr. Curnutte and built by the KSU Physics

shop. Henceforth, this detector will be referred to as the brass detector. The other conversion electron detector was provided by Dr. Kinetkar (see Figures 12 and 13), hereafter referred to as the plexiglass detector. These two detectors are flowing gas detectors requiring a helium/10%-methane gas mixture, purchased from Matheson Gas Products. The two stage regulator for the helium/methane tank was a model MOD 8L-350 regulator, also purchased from Matheson Gas Products. Due to insufficient fine control in the regulator, a Hoke needle valve with a 60° taper was inserted into the tygon tubing between the tank and the detector.

The original design of the brass detector was unable to provide an acceptable signal level due to a large separation of the sample and the anode wires (about 5 mm). At this distance, no resonance signal could be discerned from the backround. The separation was reduced to about 2 mm by using a sample mount extender that positions the sample further into the window cavity. The mount was devised and built by Dr. Curnutte. The use of this mount boosted the signal level above the backround, to a workable level. This modification however, did not bring the preformance of the brass detector up to that of the plexiglass detector. Too large a sample to anode gap allows the helium ions to undergo recombination with their

electrons before the electrons can be collected by anode wires.

The detectors were powered by a Tennelec TC 951 High Voltage Power Supply (see Table I). The detector output was fed to an Ortec 109PC preamplifier which in turn was powered by an Ortec 115 Power Supply. The preamp output pulse was sent to a Tennelec TC 200 amplifier in order to further increase the signal intensity to the level required by an Ortec 406A Single Channel Analyzer. Pulses of the desired height were selected by setting the upper and lower windows of the latter. Once such a pulse was detected, the SCA emitted a 5 V pulse to initiate a computer D/A conversion in the of the source Doppler motion.

Data Collection:

When the signal from the single channel analyzer was received by the AI-13 board (Interactive Microware) in an Apple IIe computer, also purchased from Interactive Microware, sampling and conversion (20 μs) of the voltage put out by the Doppler frequency generator was begun. Upon completion of the D/A conversion, the converter raised an interrupt flag on the Apple IIe bus. This acted as a signal to the resident program CONVEL.OBJ, written by Dr. Keith Purcell in Apple Assembly, to increment the photon count of the address

corresponding to the most significant 8 bits of the 12 bit A/D output. At this point, the interrupt flag was cleared and the AI-13 board was allowed to accept another signal from the single channel analyzer. This process continued until one of the photon count addresses reached an operator-selectable, predetermined value, at which time data collection is automatically terminated.

Data Handling

Due to the biases in the A/D converter reference voltage ranges, it was necessary to divide, point by point, a normalized sample spectrum by a normalized base-line spectrum. The corrected spectrum was then scaled back to the level of the original sample spectrum. This program, SPECSCALER, was written in Apple BASIC by Dr. Keith Purcell. It has two additional functions, the first of which is to produce a data file scaled to be used by STRIPCHARTER (a plotting program supplied by Interactive Microware) to produce a plot on an Epson RX-80 Dot Matrix Printer (purchased from Interactive Microware). The second function is invert the corrected spectrum for conversion electron Mossbauer experiment so that it may be fit and plotted using the program MOSSFIT (written in FORTRAN by the Mossbauer group at Johns Hopkins and locally modified by Dr. Keith

Purcell) resident on the campus computer system.

System Calibration

The system was calibrated using several spectra, the first of which (Figure 14) consisted of the inner two lines of an enriched ^{57}Fe foil. Following this, (Figures 15 to 17) natural abundance stainless steel foil spectra were taken with each detector to evaluate their preformance. The final calibration spectrum was a basline spectrum. This last spectrum (Figure 18) is included to show that the random scatter is fairly close to the theoretical limit of 1/2 %.

Table I. Optimal Settings for the Tennelec TC 200 Amplifier and the Ortec 406 A Single Channel Analyzer for Each Detector.

Dial name	Settings		
	Trans.	brass	plexi.
Course Gain	16	8	1
First Differentiator	16	16	16
Integrator	0.4	1.6	1.6
Second Differentiator	3.2	3.2	3.2
Fine Gain	0.6	0.95	0.95
Polarity	Direct	Direct	Direct
Power	1750 V	1250 V	1250 V
SCA Window settings			
Upper	0.40	3.24	1.00
Lower	0.12	1.14	0.22

Figure 4

Exploded view of the outer case of the brass conversion electron detector.

A. Top lid, brass. Not shown: MHV connector through center hole; 4 screws, size 4-40, for the corner holes.

B. Rubber gasket.

C. Two piece detector body, brass. Not shown: 2 gas nipples, hard plastic, for 1/4" holes. These are similar to the straight connectors offered by Dynalab; inner unit (Figure 8); window adapter unit, Fe-free aluminum; 2 rubber O-rings, 7/8" od., 1/16" thick; Mylar or Fe-free aluminum window covers.

D. Threaded window insert, brass. Not shown: two holes on the outer face, 3/32" dia., 3/16" deep. These allow a key to be used to unscrew or tighten down the unit.

E. Rubber gasket.

F. Bottom lid, brass. Not shown: 4 screws, size 4-40, for the corner holes.

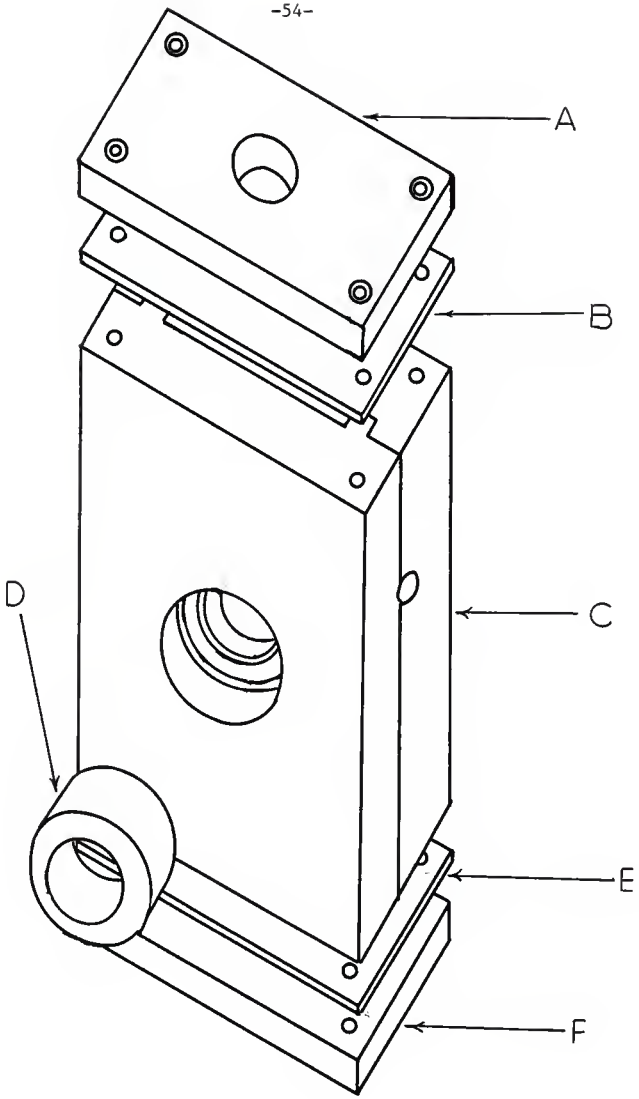
A
B
C
D
E
F

Figure 5

Front view of detector outer case.

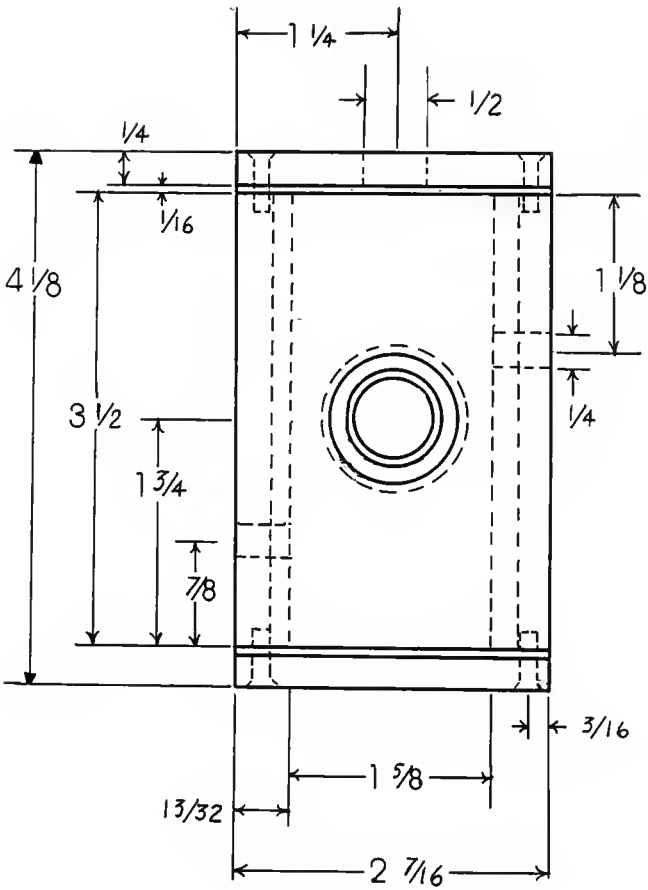
1 1/4
1/2
1/4
1/16
4 1/8
1 1/8
3 1/2
1/4
1 3/4
7/8
3/16
1 5/8
13/32
2 7/16

Figure 6

Side view of detector outer case.

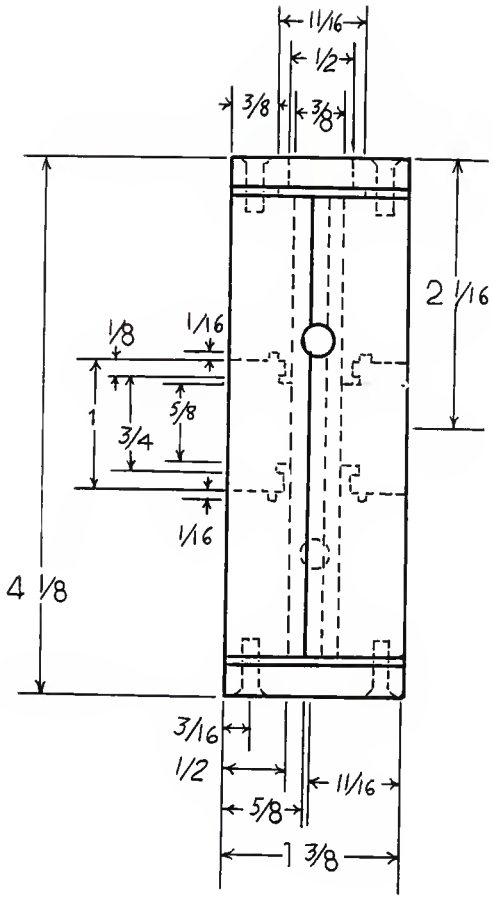
1 1/16
1/2
3/8
3/8
2 1/16
1/8
1/16
5/8
1
3/4
1/16
4 1/8
3/16
1/2
1 1/16
5/8
1 3/8

Figure 7

Top view of the detector outer case.

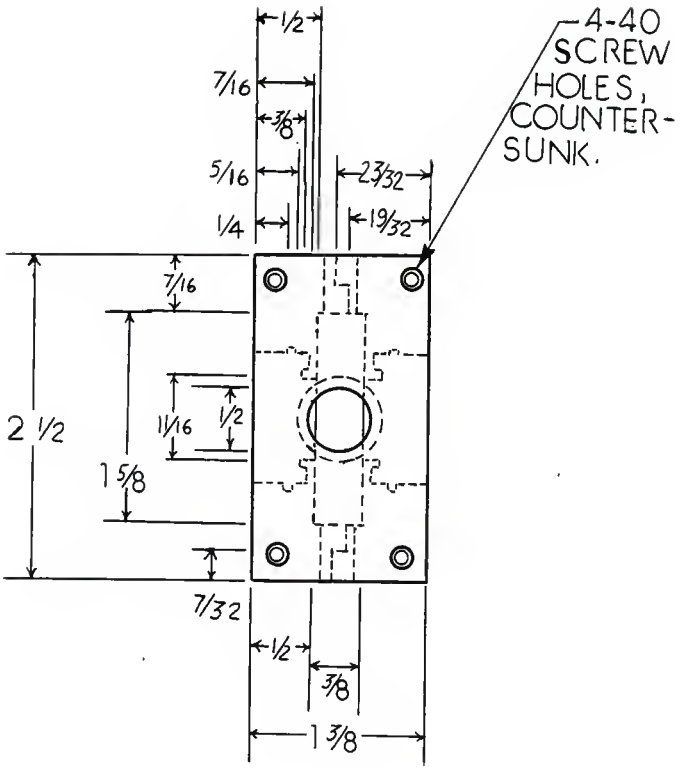
1/2
7/16
3/8
5/16
23/32
1/4
19/32
4-40 SCREW HOLES, COUNTER-SUNK.
7/16
2 1/2
11/16
1/2
1 5/8
7/32
1/2
3/8
1 3/8

Figure 8

Exploded view of the inner unit of the brass detector.

A. Screws, aluminum; size 3-36.
B. Wire holder, brass. Size 1 1/8" X 1/4" X 1/16" with holes for the screws and the detector wires (not shown).
C. Inner unit body, polyurethane.
D. Springs, 3/16" dia.
E. Wire holder, brass. Size 1 1/2" X 1/4" X 1/16" with 1/4" dia. rounded ends and holes for the detector wire.

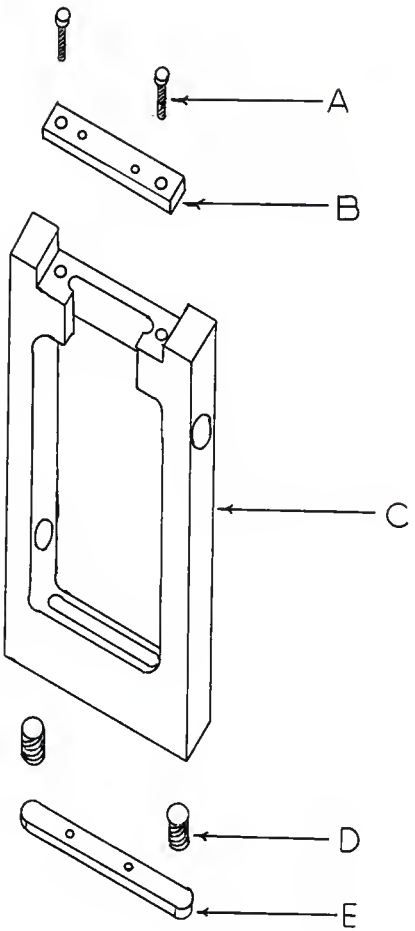
A
B
C
D
E

Figure 9

Front view of detector inner unit.

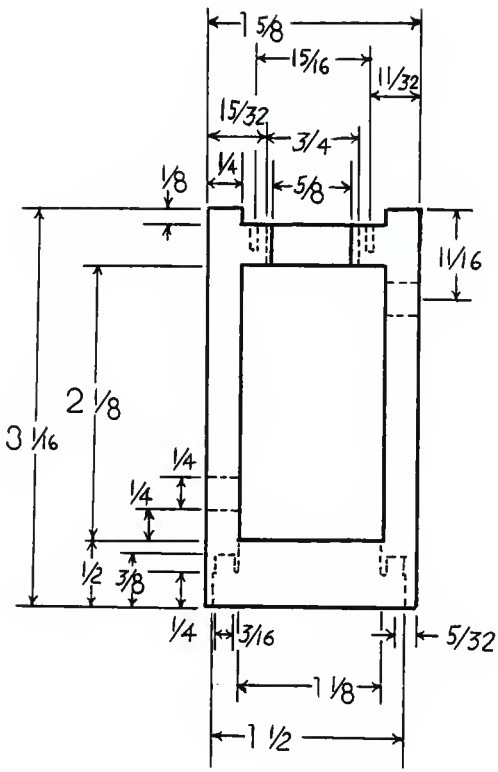
1 5/8
15/16
11/32
15/32
3/4
1/4
5/8
1/8
11/16
3 1/16
2 1/8
1/4
1/4
1/2
3/8
1/4
3/16
5/32
1 1/8
1 1/2

Figure 10

Side view of detector inner unit.

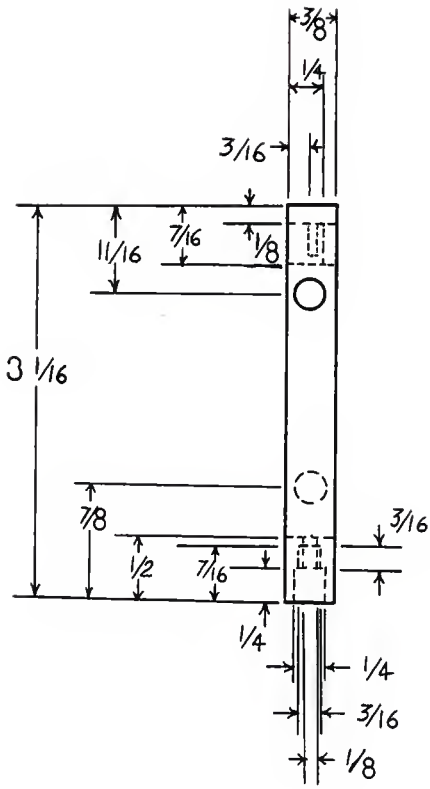
3/8
1/4
3/16
7/16
1/8
11/16
3 1/16
7/8
1/2
7/16
3/16
1/4
1/4
3/16
1/8

Figure 11

Top view of detector inner unit.

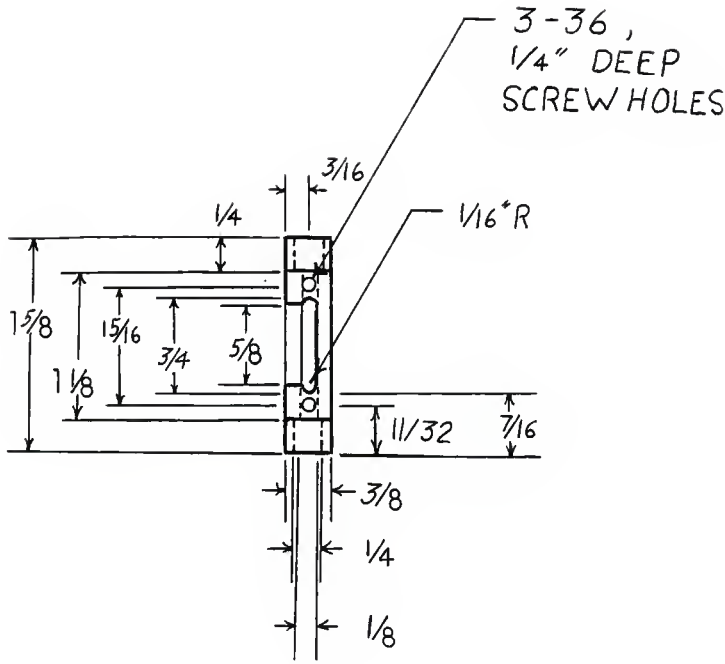
3-36,
1/4" DEEP
SCREW HOLES
3/16
1/4
1/16"R
1 5/8
15/16
3/4
5/8
1 1/8
11/32
7/16
3/8
1/4
1/8

Figure 12

Front view of the plexiglass detector.

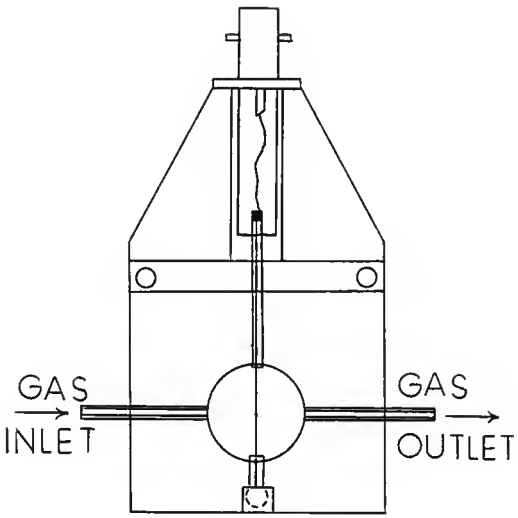
GAS
INLET
GAS
OUTLET

Figure 13

Side view of the plexiglass detector.

A. MHV connector.

B. Teflon.

C. Hypodermic needle.

D. Anode wire.

E. Sample.

F. Be or Mylar window.

G. Glass insulator.

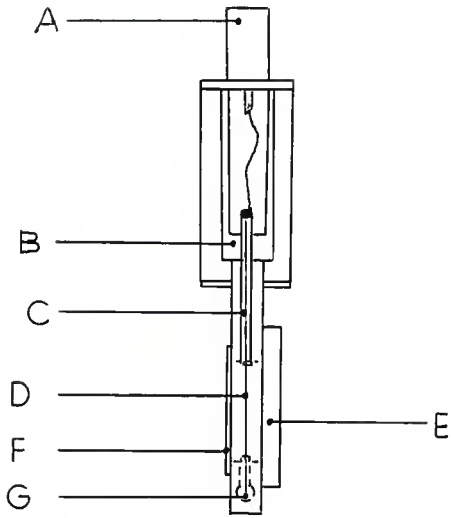
A
B
C
D
E
F
G

Figure 14

Transmission Mossbauer spectrum of enriched iron foil.

IRON FOIL CALIBRATION 2/18/87

COUNTS =50575. OPT=UNC

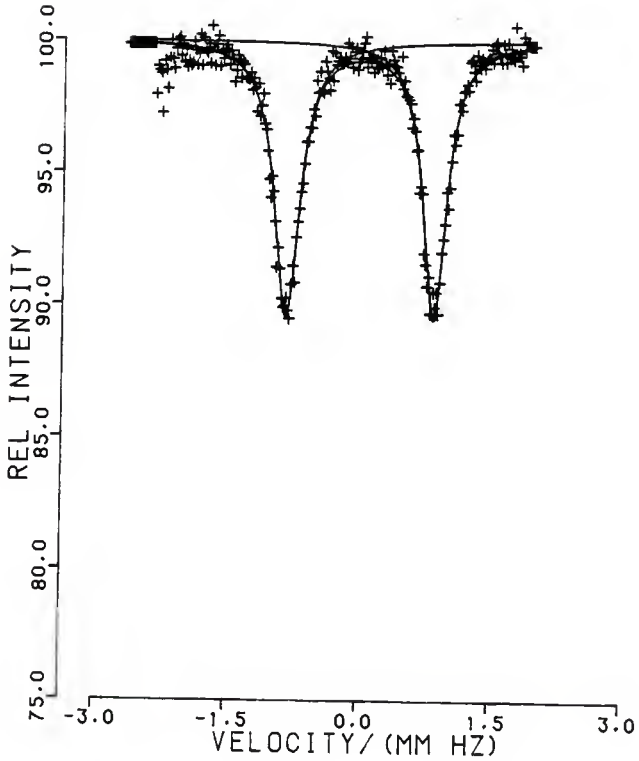

Figure 15

Transmission Mossbauer spectrum of natural abundance stainless steel foil.

TRANSMISSION SPECTRUM
STAINLESS STEEL FOIL 2/18/87
COUNTS =50236. OPT=UNC

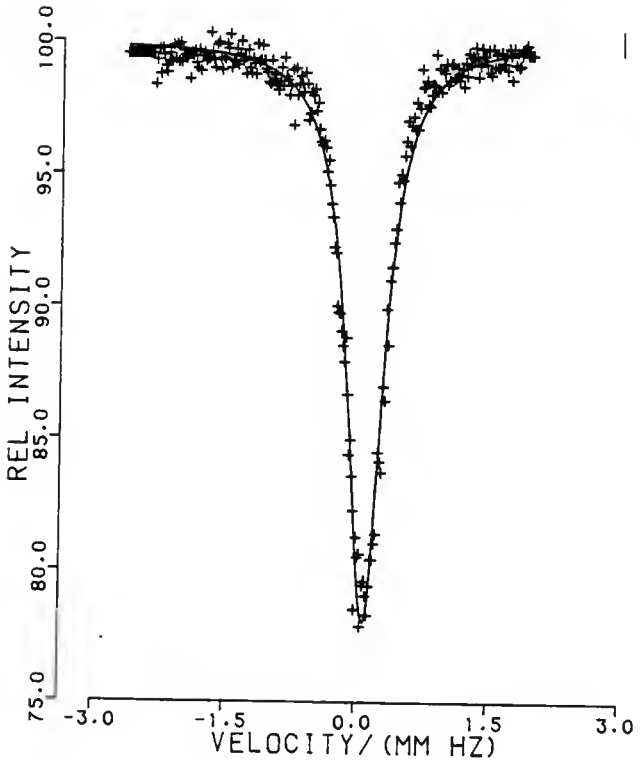

Figure 16

Conversion Electron Mossbauer spectrum of natural abundance stainless steel foil using the plexiglass detector.

CEMS SPECTRUM. PLEXIGLASS DETECTOR
STAINLESS STEEL FOIL 1/20/87
COUNTS =48665. OPT=UNC

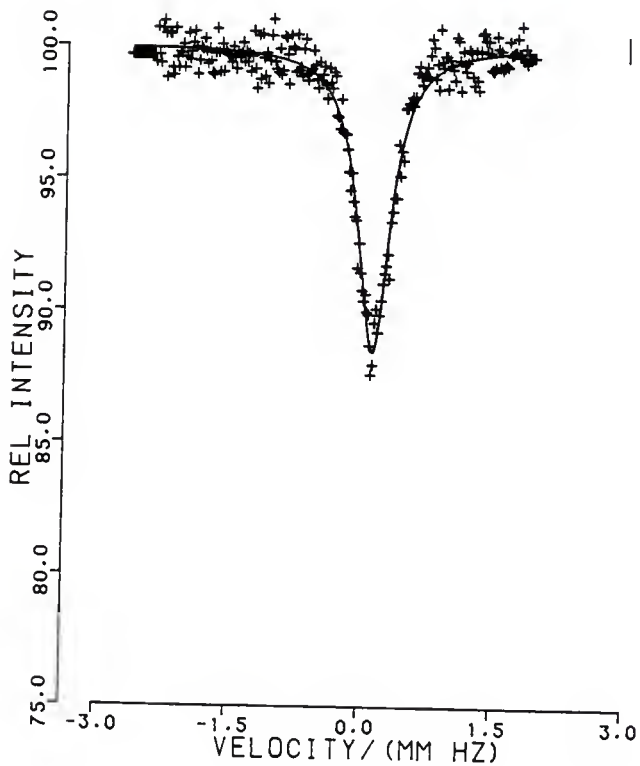

Figure 17

Conversion Electron Mossbauer spectrum of natural abundance stainless steel foil using the brass detector.

CEMS SPECTRUM, BRASS DETECTOR
STAINLESS STEEL FOIL
COUNTS =47140. OPT=UNC

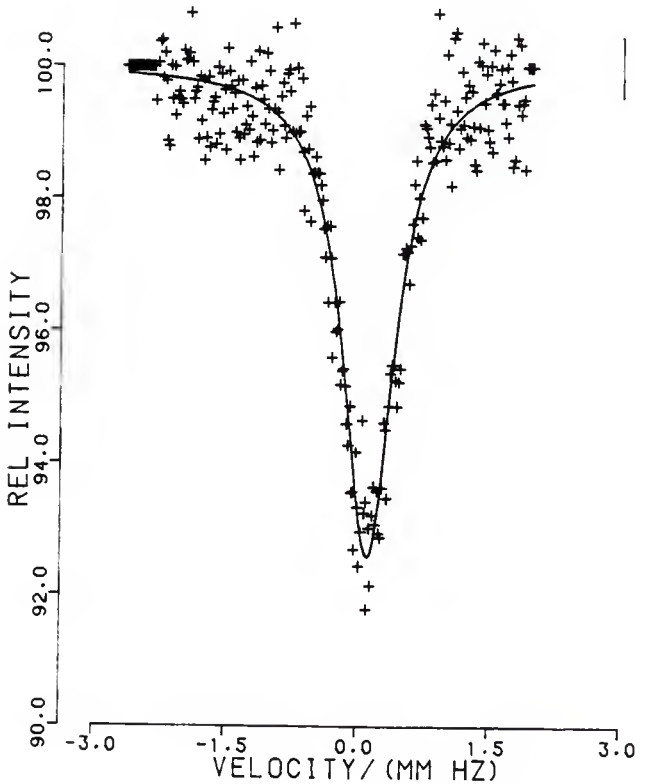

Figure 18

Baseline spectrum collected by Transmission Mossbauer Spectroscopy.

BASELINE SPECTRUM. NO SAMPLE
SPECTRUM RUN 2/23/87
COUNTS =0. OPT=NFIT

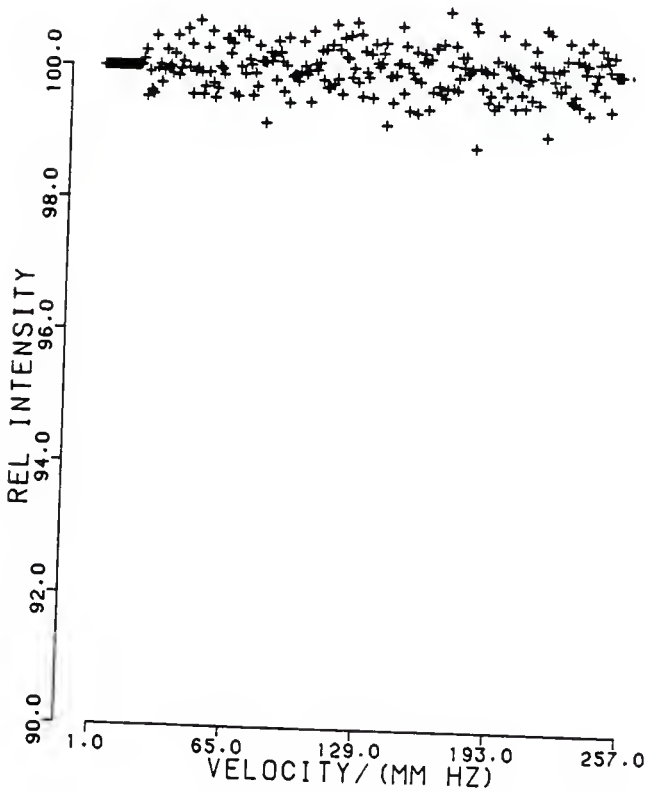

RESULTS

Infrared Spectroscopy. The infrared spectra for all the compounds prepared are very complex and do not lend themselves to easy interpretation. However, the spectra can be used to identify the anions in the BPh_4^- and PF_6^- salts. As seen in Figures 19 and 20, for BPh_4^- salts there is a strong-medium intensity peak at about 708 cm^{-1},[52] while the PF_6^- salts exhibit a peak of medium intensity at about 550 cm^{-1}.[51]

Electron Paramagnetic Resonance Spectroscopy. The ESR spectra (Figures 21 to 30) give only limited information because minor peaks are often either nearly buried by broad major peaks or are visible only as shoulders on the side of a peak. All of the compounds exhibit resonances at $g \sim 4.3$ which be assigned to a high spin d^5 resonance, as discussed by Drago.[53] Likewise, the shoulder and side peaks that fall in the range of g = 5 to 9 can also be assigned to the high spin molecules. The resonances at $g \sim 2$ may be due to the low spin fraction. However, it is clear from our data that the completely high-spin complexes (Figures 21,23,24 and 27) have a significant resonance at $g \sim 2$, that is at times as large or larger than the resonance at $g \sim 4.3$. See Table II for the g values of the compounds.

Figure 19

Infrared spectrum of $[Fe(py)L]BPh_4$; nujol mull.

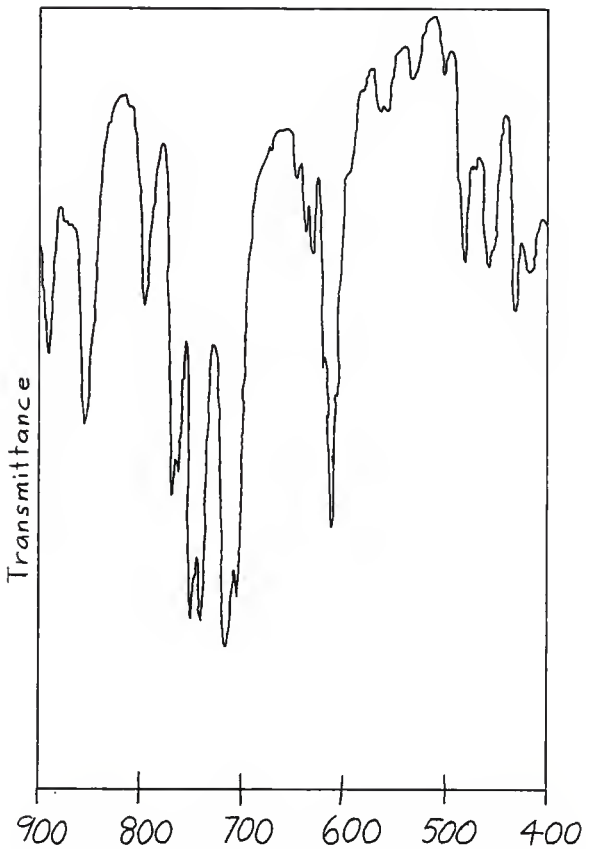
Transmittance
900
800
700
600
500
400

Figure 20

Infrared spectrum of $[Fe(py)L]PF_6$; CCl_4 mull.

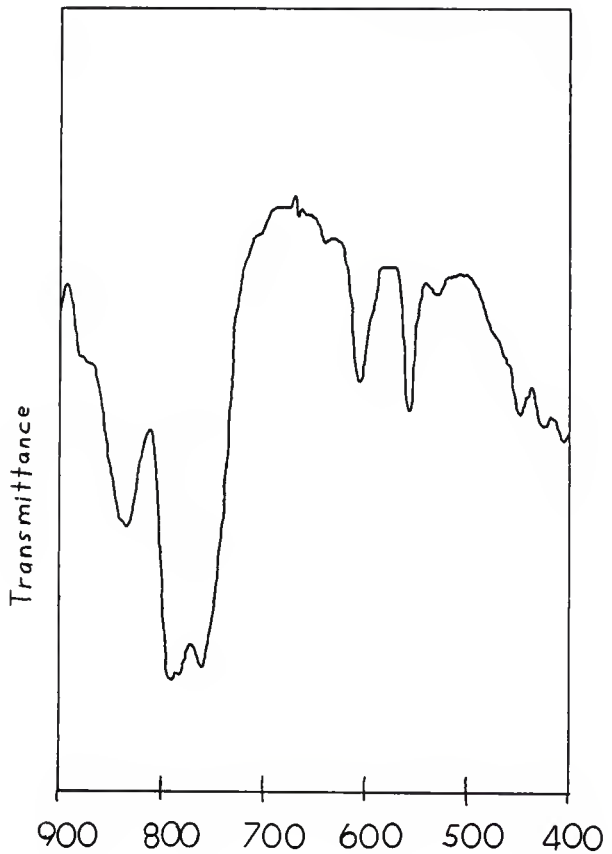
Transmittance
900
800
700
600
500
400

Figure 21

Electron Paramagnetic Resonance spectrum of [Fe(Cl)L].

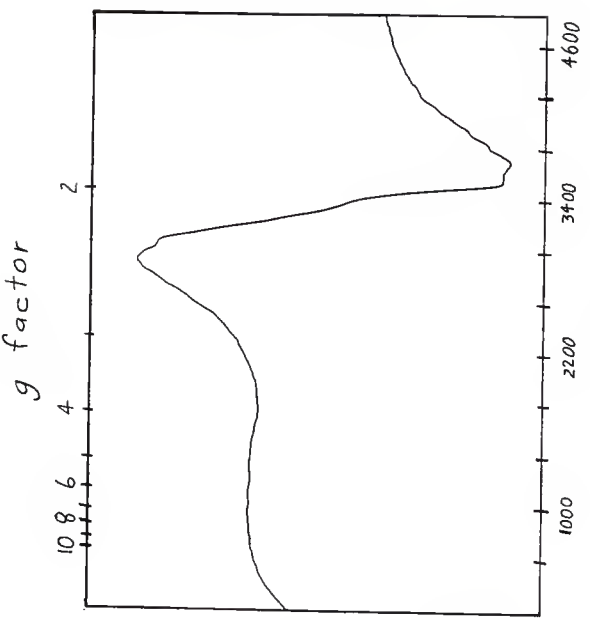
g factor
10
8
6
4
2
1000
2200
3400
4600
Gauss

Figure 22

Electron Paramagnetic Resonance spectrum of $[Fe(3Me\text{-}py)L]BPh_4$.

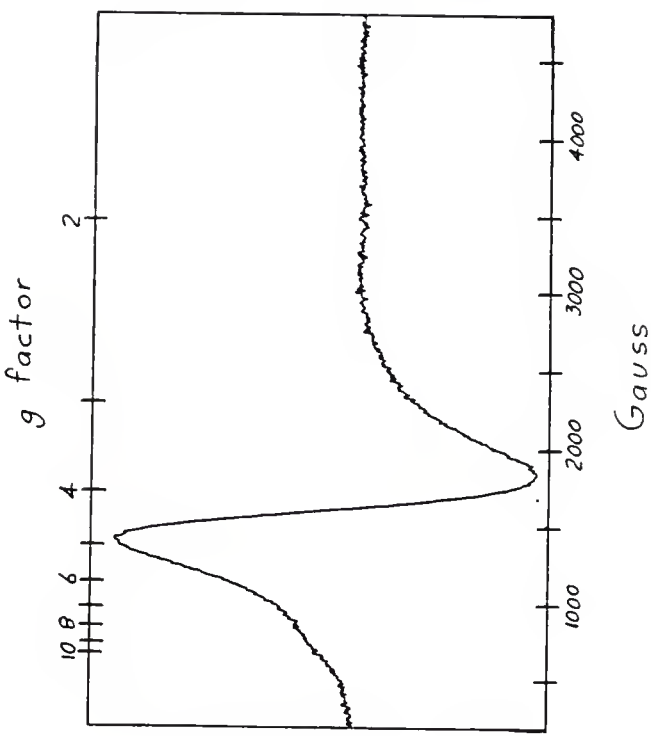
g factor
10
8
6
4
2
1000
2000
3000
4000
Gauss

Figure 23

Electron Paramagnetic Resonance spectrum of $[Fe(NA)L]BPh_4$.

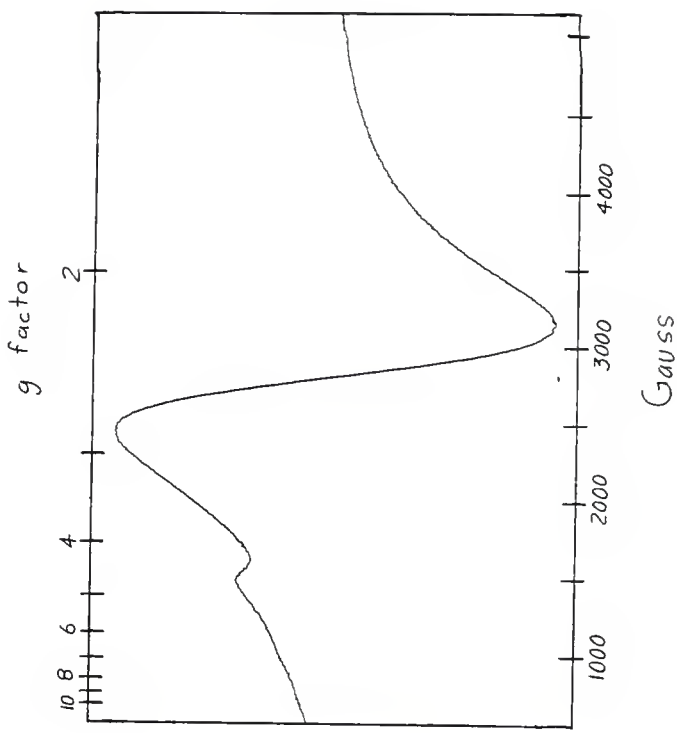
g factor
10
8
6
4
2
1000
2000
3000
4000
Gauss

Figure 24

Electron Paramagnetic Resonance spectrum of [Fe(NA)L]Cl.

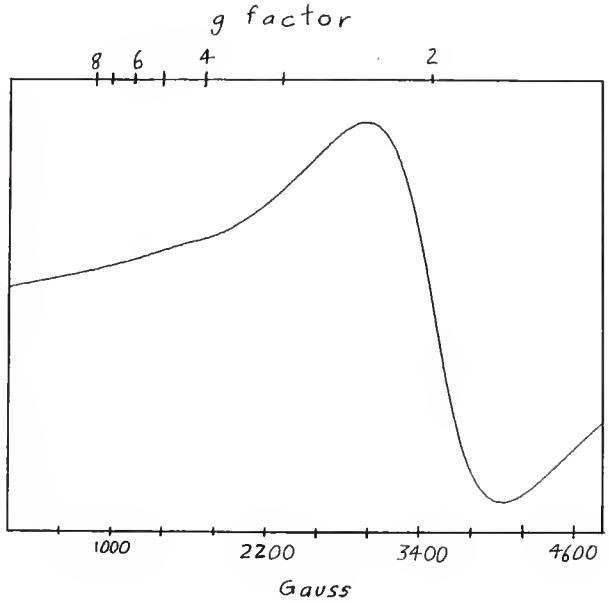
g factor
8
6
4
2
1000
2200
3400
4600
Gauss

Figure 25

Electron Paramagnetic Resonance spectrum of $[Fe(3,4Me_2\text{-py})L]BPh_4$.

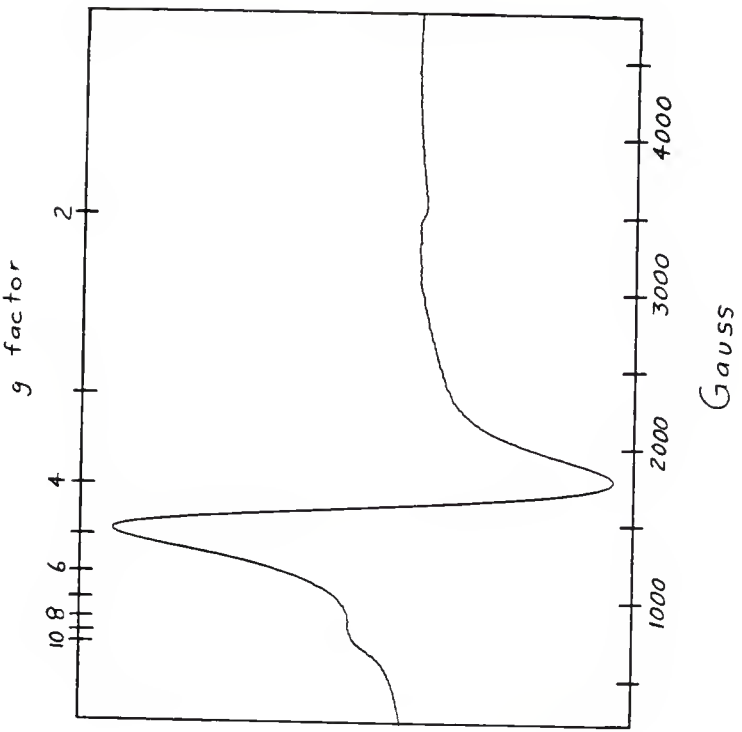
g factor
10
8
6
4
2
1000
2000
3000
4000
Gauss

Figure 26

Electron Paramagnetic Resonance spectrum of $[Fe(DPA)L]BPh_4$.

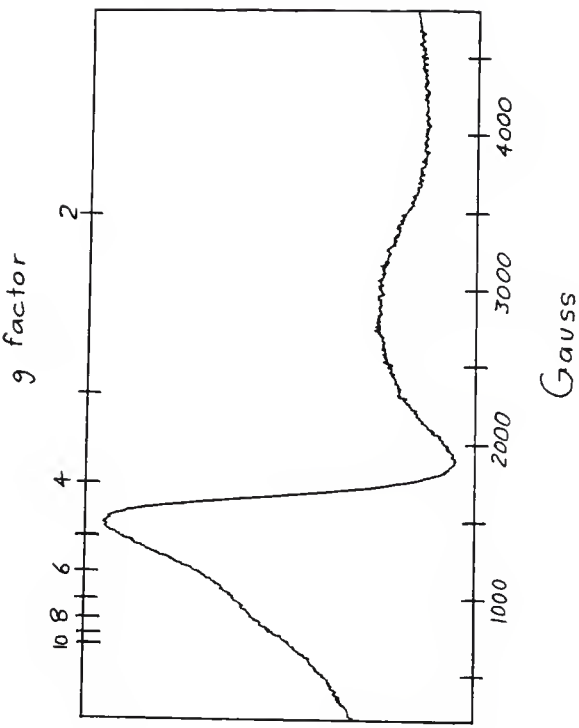
g factor
10
8
6
4
2
1000
2000
3000
4000
Gauss

Figure 27

Electron Paramagnetic Resonance spectrum of [Fe(DPA)L]Cl.

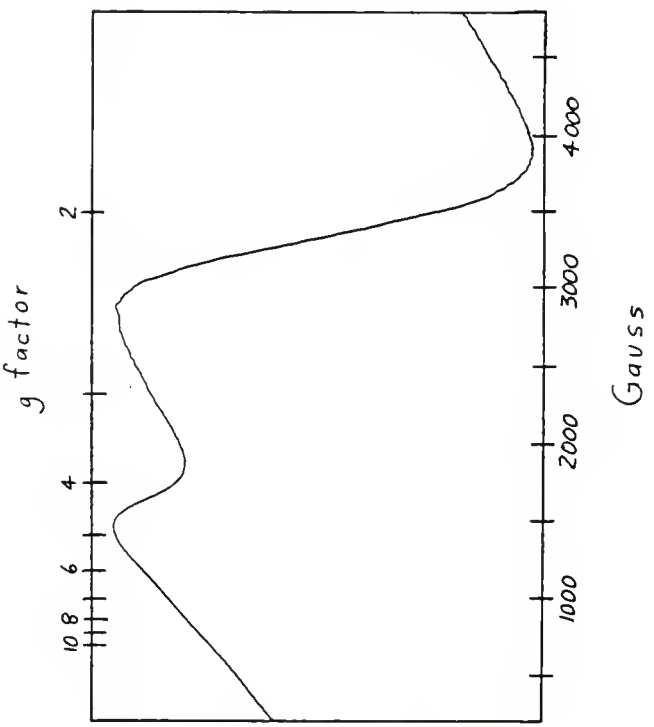
g factor
10
8
6
4
2
1000
2000
3000
4000
Gauss

Figure 28

Electron Paramagnetic Resonance spectrum of $[Fe(py)L]BPh_4$.

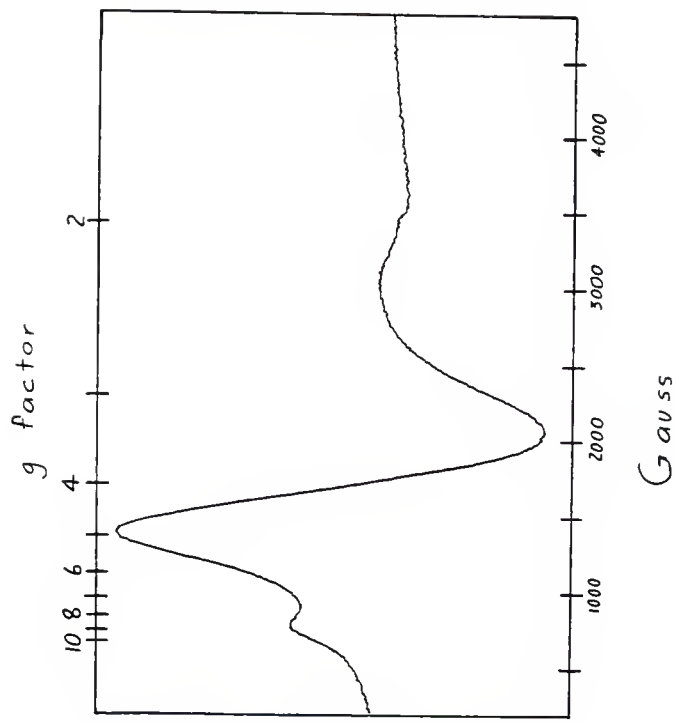
g factor
10
8
6
4
2
1000
2000
3000
4000
Gauss

Figure 29

Electron Paramagnetic Resonance spectrum of $[Fe(py)L]PF_6$.

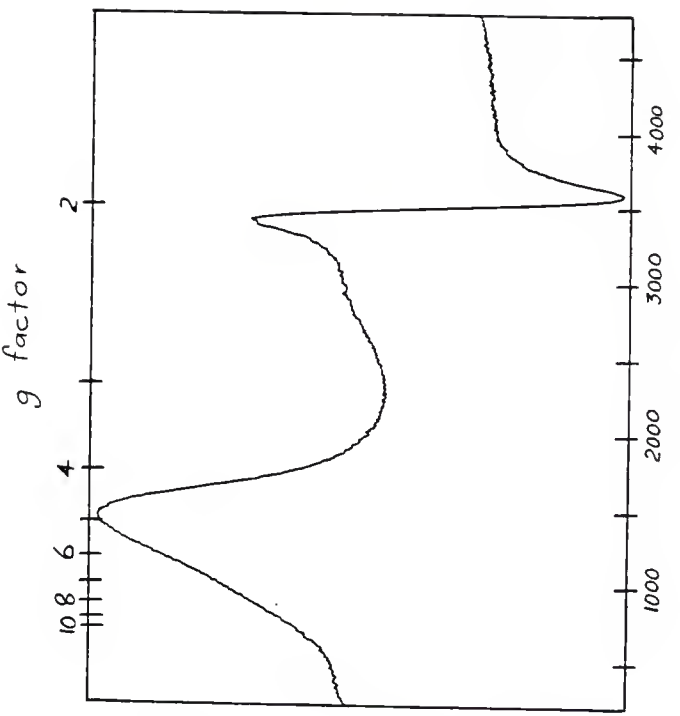
g factor
10
8
6
4
2
1000
2000
3000
4000
Gauss

Figure 30

Electron Paramagnetic Resonance spectrum of $[Fe(O\text{-}py)L]BPh_4$.

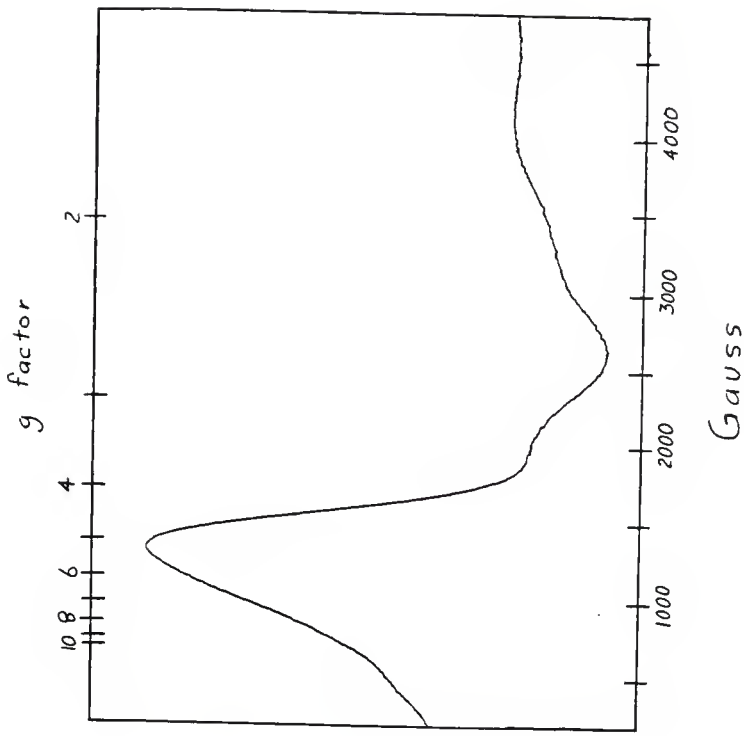
g factor
10
8
6
4
2
1000
2000
3000
4000
Gauss

Table II. g-values calculated from Electron Paramagnetic Resonance Spectra.

Compound	major peak	minor peaks
[Fe(Cl)L]	2.10	3.98
[Fe(3Me-py)L]BPh_4	4.21	7.66
[Fe(NA)L]BPh_4	2.03	4.27
[Fe(NA)L]Cl	2.01	4.03
[Fe(3,4Me_2-py)L]BPh_4	4.31	8.32, 2.00
[Fe(DPA)L]BPh_4	4.22	2.03
[Fe(DPA)L]Cl	2.10, 4.26	
[Fe(py)L]BPh_4	4.18	2.09, 7.74
[Fe(py)L]PF_6	4.12	2.00
[Fe(O-py)L]BPh_4	4.38	2.62, 2.10

Note: Nearly every compound has a buried or partially buried resonance around g = 6 to 9. The major peak assignments have been made by comparative height since the spectra exhibit severe overlapping of resonances.

Table III. μ_{eff} Data for $[Fe(X)L]^{+n}$ [a]

(n = 0,1) and Related Compounds.

Compound	Experimental		Estimated f_Q [b]
	μ_{eff}	Temp	
$[Fe(Cl)L]^{i}$	5.86(4)	299	1.
$[Fe(3Me\text{-}py)L]BPh_4$ [ii]	4.45(6)	301	.6
$[Fe(NA)L]BPh_4$ [d]	6.29(6)	295.5	1.
$[Fe(NA)L]Cl$ [d]	7.16(5)	295.5	-
$[Fe(3,4Me_2\text{-}py)L]BPh_4$ [iii]	3.9 (1)	301	.5
$[Fe(DPA)L]BPh_4$ [e]	4.15(6)	295.5	.5
$[Fe(DPA)L]Cl$ [e]	5.8 (1)	297.5	1.
$[Fe(py)L]BPh_4$ [iv]	4.19(8)	301	.5
$[Fe(py)L]PF_6$	5.04(5)	297.5	.8
$[Fe(O\text{-}py)L]BPh_4$ [c]	6.56(3)	301	1.

a μ and T values from reference 46: (i) 5.82, 298; (ii) 4.39, 297; (iii) 4.10, 305 (iv) 4.18, 297.

b Calculated from μ_{ls} = 2. and μ_{hs} = 6.

c O-py = pyridine N-oxide

d NA = nicotinic acid

e DPA = 3,4-dipicolinic acid

Mossbauer Spectroscopy. The original Mossbauer transmission spectra for the compounds presented in this work were relatively weak and thus had relatively low signal:noise ratios. The reason for this is most likely the low areal densities of ^{57}Fe in the fluffy solids (densities 0.8 g/cm^3). Packing of the solids in a tube increased the signals from essentially basline (0.5 %) to appreciable levels (3 to 4 %). These spectra are given in Figures 31 to 39 and with the exception of $[Fe(3,4Me_2\text{-py})L]BPh_4$ they have all been fit with a two independent Lorentzian lines. A transmission spectrum could not be obtained from $[Fe(DPA)L]BPh_4$, most likely due to a combination of a low areal density and a low recoilless fraction. As noted in the experimental section, the brass conversion electron detectors did not produce as large a signal:noise ratio as did the plexiglass detector.

Figure 31

Transmission Mossbauer spectrum of [Fe(Cl)L].

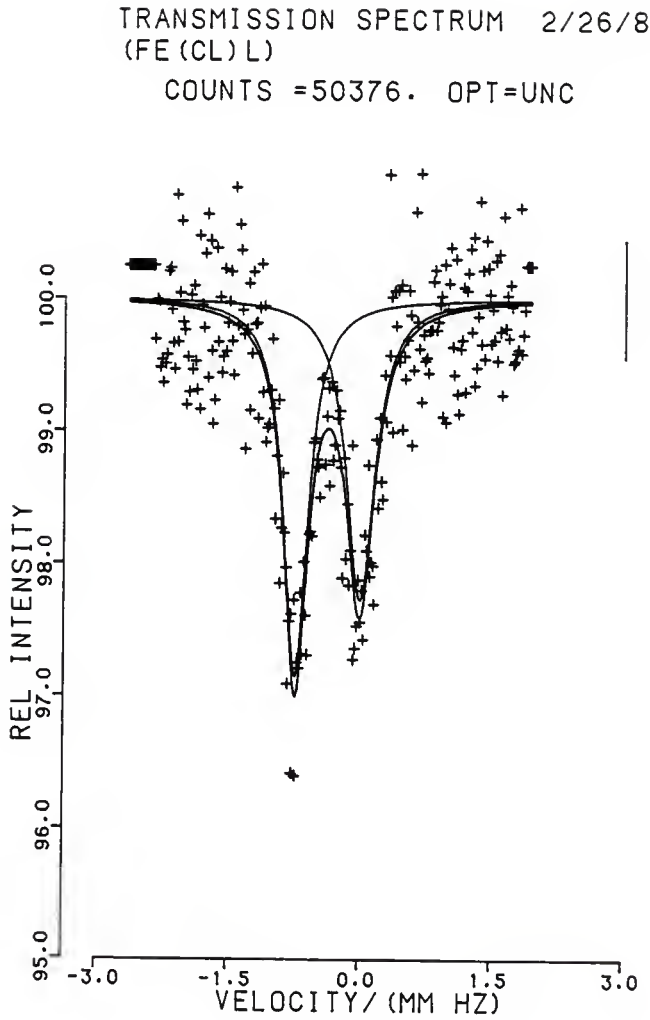
TRANSMISSION SPECTRUM 2/26/87
(FE(CL)L)
COUNTS =50376. OPT=UNC
REL INTENSITY
100.0
99.0
98.0
97.0
96.0
95.0
-3.0
-1.5
0.0
1.5
3.0
VELOCITY/(MM HZ)

Figure 32

Transmission Mossbauer spectrum of $[Fe(3Me\text{-}py)L]BPh_4$.

TRANSMISSION SPECTRUM 2/26/87
(FE(3ME-PY)L)BPH4
COUNTS =50505. OPT=UNC

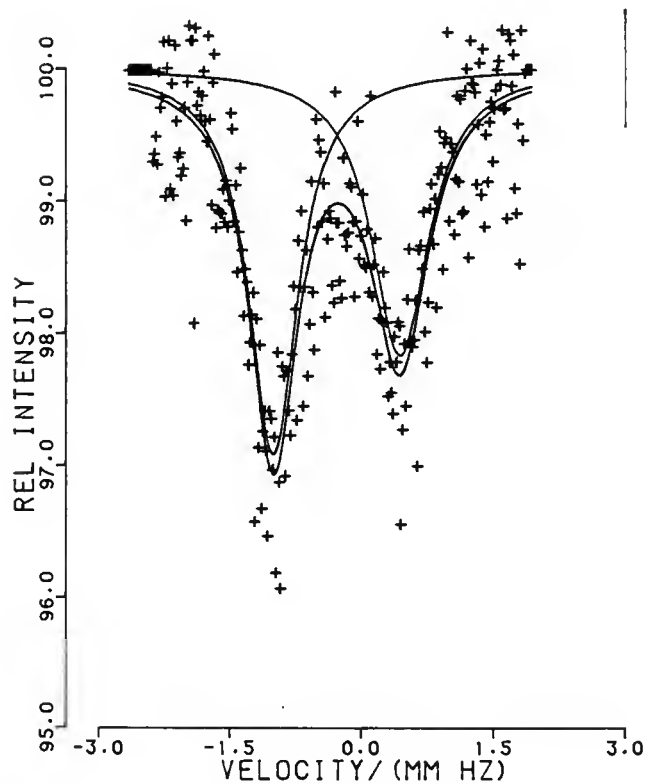

Figure 33

Transmission Mossbauer spectrum of $[Fe(NA)L]BPh_4$.

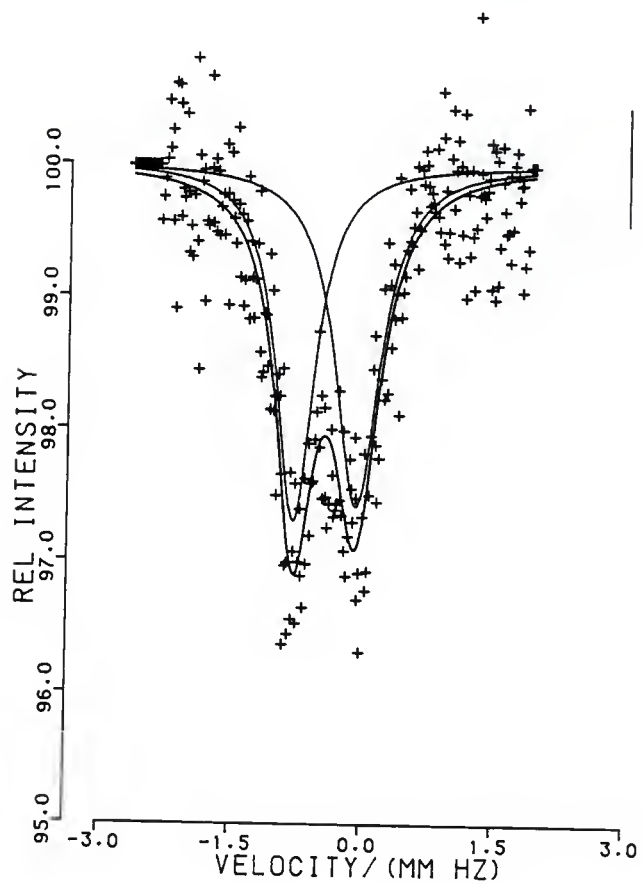
TRANSMISSION SPECTRUM 2/26/87
(FE (NA) L) BPH4
COUNTS =50207. OPT=UNC
REL INTENSITY
100.0
99.0
98.0
97.0
96.0
95.0
-3.0
-1.5
0.0
1.5
3.0
VELOCITY/ (MM HZ)

Figure 34

Transmission Mossbauer spectrum of [Fe(NA)L]Cl.

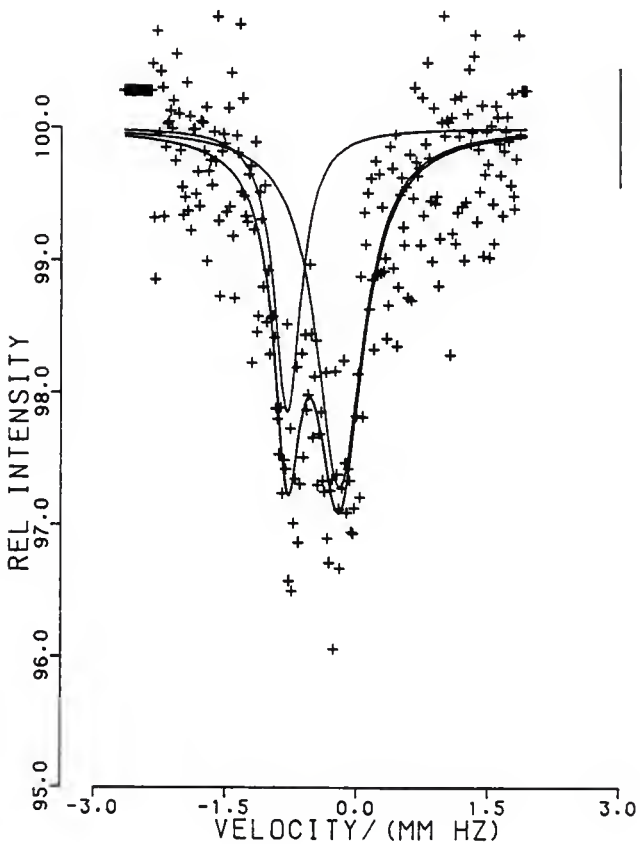
TRANSMISSION SPECTRUM 2/26/87
(FE(NA)L)CL
COUNTS =50061. OPT=UNC
REL INTENSITY
100.0
99.0
98.0
97.0
96.0
95.0
-3.0
-1.5
0.0
1.5
3.0
VELOCITY/(MM HZ)

Figure 35

Transmission Mossbauer spectrum of $[Fe(3,4Me_2\text{-py})L]BPh_4$; two line fit.

TRANSMISSION SPECTRUM RUN 2/24/87
(FE(3,4ME2-PY)L)BPH4 NAT. ABD.
COUNTS =50552. OPT=UNC

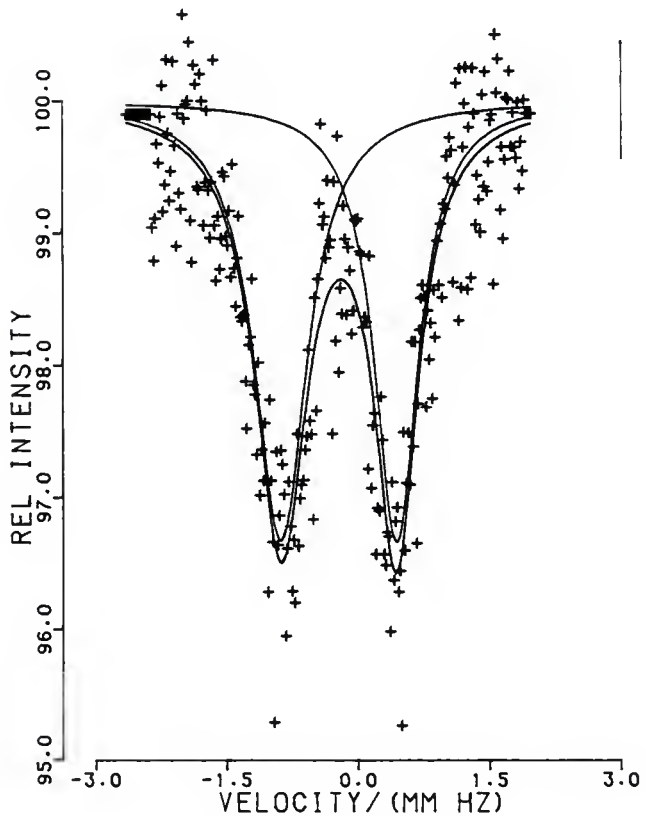

Figure 36

Transmission Mossbauer spectrum of $[Fe(3,4Me_2\text{-py})L]BPh_4$; three line fit.

TRANSMISSION SPECTRUM RUN 2/24/87
(FE(3,4ME2-PY)L)BPH4 NAT. ABD.
COUNTS =50532. OPT=UNC

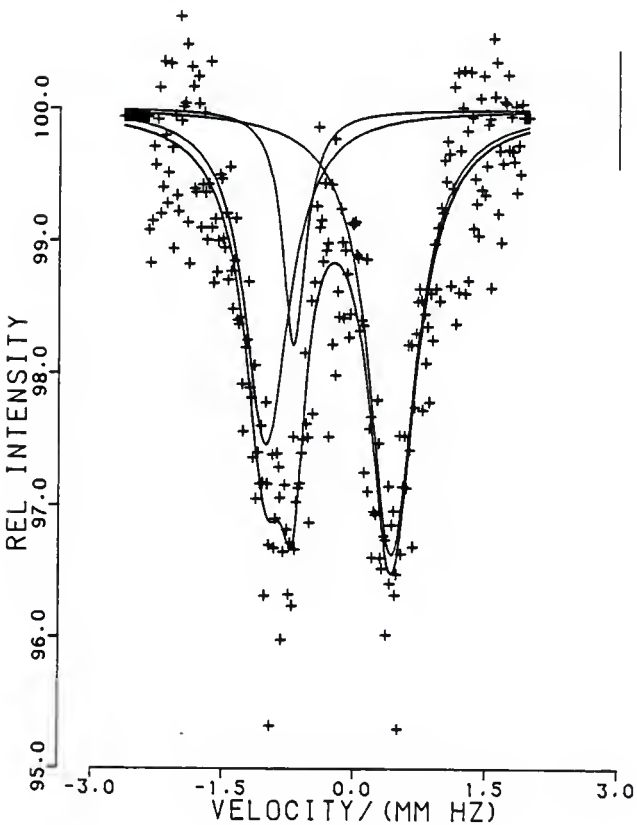

Figure 37

Transmission Mossbauer spectrum of $[Fe(3,4Me_2\text{-py})L]BPh_4$; four line fit.

TRANSMISSION SPECTRUM RUN 2/24/87
(FE(3,4ME2-PY)L)BPH4 NAT. ABD.
COUNTS =50534. OPT=UNC

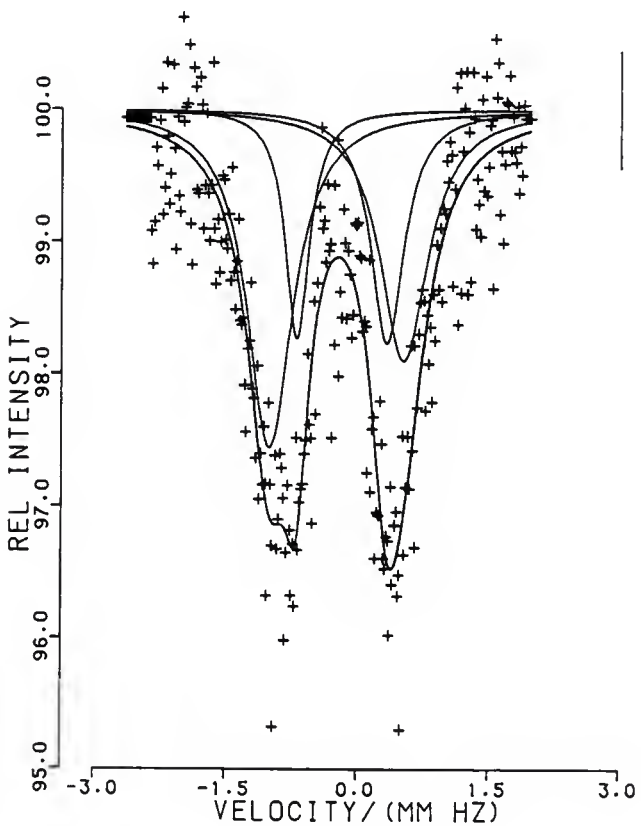

Figure 38

Transmission Mossbauer spectrum of [Fe(DPA)L]Cl.

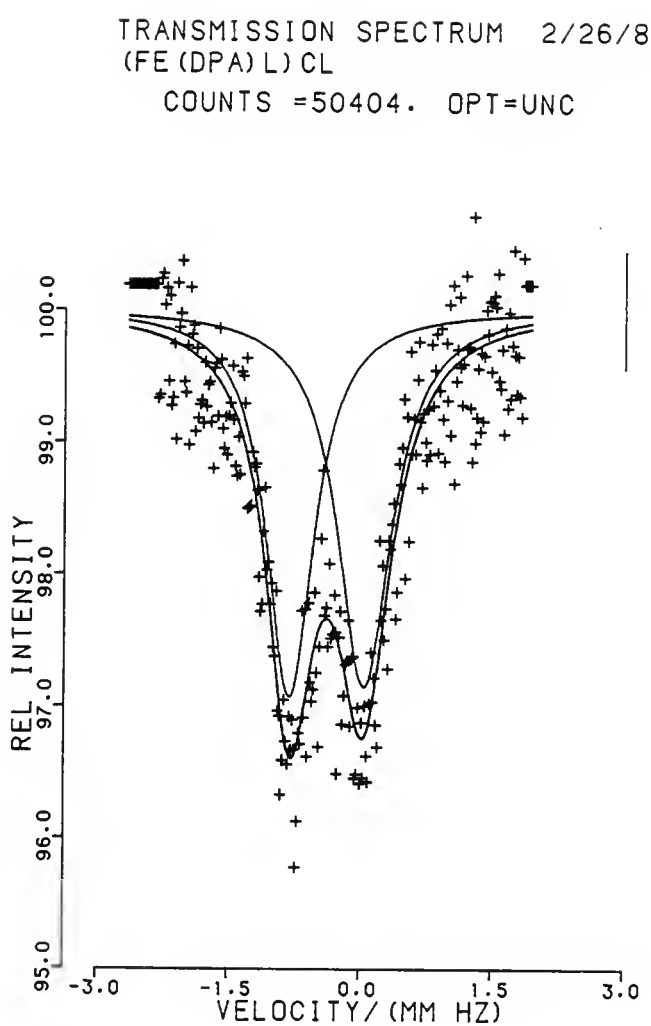
TRANSMISSION SPECTRUM 2/26/87
(FE(DPA)L)CL
COUNTS =50404. OPT=UNC
REL INTENSITY
100.0
99.0
98.0
97.0
96.0
95.0
-3.0
-1.5
0.0
1.5
3.0
VELOCITY/(MM HZ)

Figure 39

Transmission Mossbauer spectrum of $[Fe(py)L]BPh_4$.

TRANSMISSION SPECTRUM 2/26/87
(FE(PY)L)BPH4
COUNTS =50405. OPT=UNC

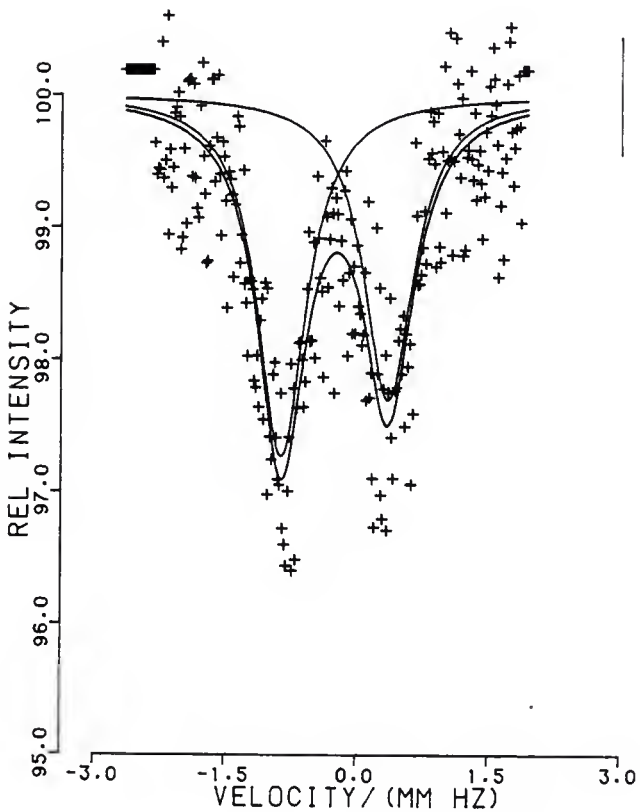

Figure 40

Transmission Mossbauer spectrum of $[Fe(py)L]PF_6$.

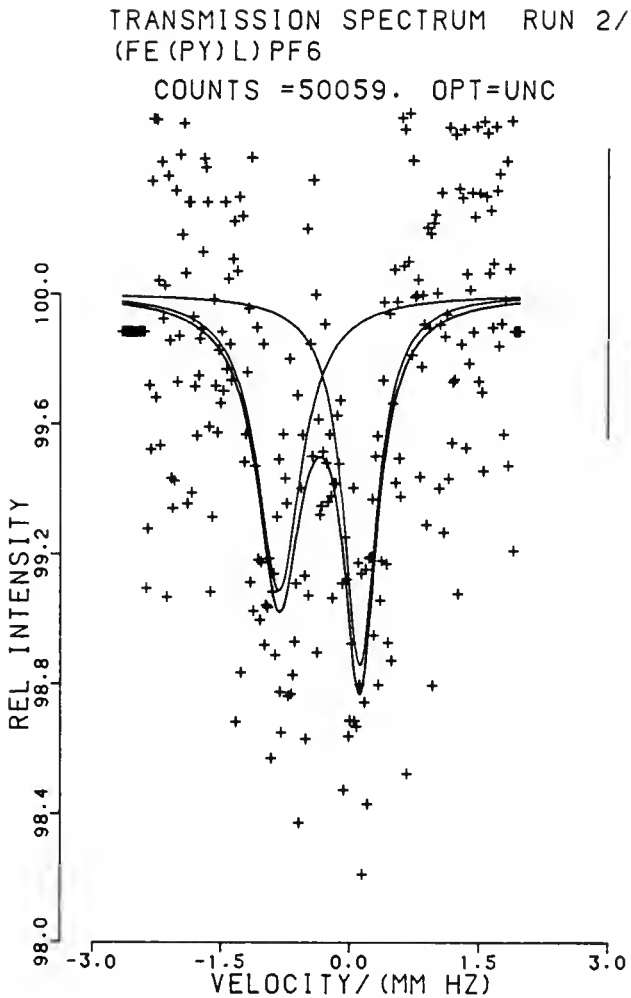
TRANSMISSION SPECTRUM RUN 2/26/87
(FE(PY)L)PF6
COUNTS =50059. OPT=UNC
REL INTENSITY
100.0
99.6
99.2
98.8
98.4
98.0
-3.0
-1.5
0.0
1.5
3.0
VELOCITY/(MM HZ)

Figure 41

Transmission Mossbauer spectrum of $[Fe(O\text{-}py)L]BPh_4$.

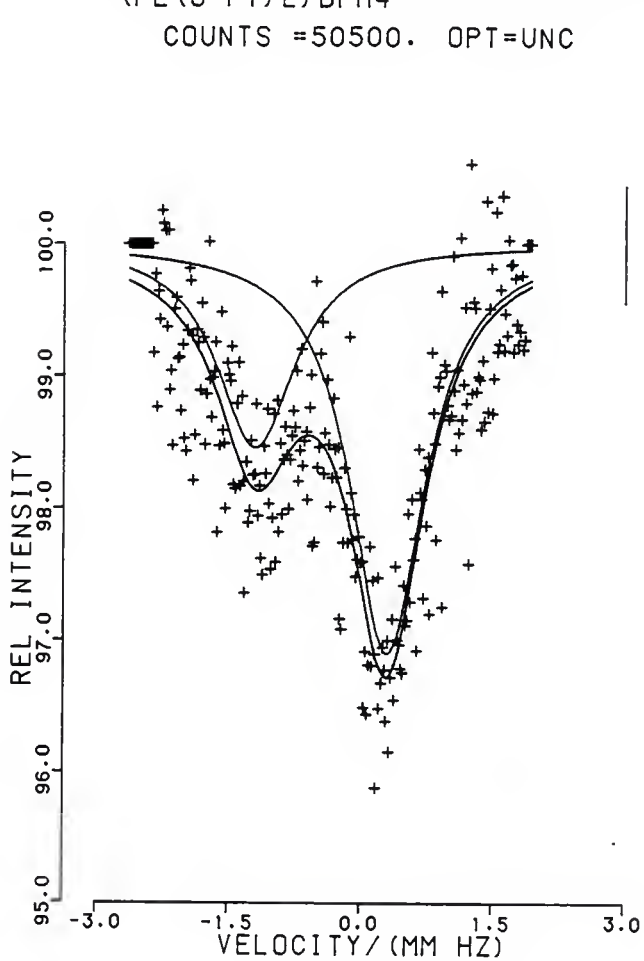
TRANSMISSION SPECTRUM 2/26/87
(FE(O-PY)L)BPH4
COUNTS =50500. OPT=UNC
REL INTENSITY
100.0
99.0
98.0
97.0
96.0
95.0
-3.0
-1.5
0.0
1.5
3.0
VELOCITY/(MM HZ)

DISCUSSION

Our investigation into one's abilty to vary the magnetic properties of spin-crossover compounds began with two analogs of the primary complex [Fe(X)L]A, where X = py and A = BPh_4^-. With the intention of lowering T_c, the first modification consisted of replacing pyridine with pyridine N-oxide. As expected, the room temperature magnetic moment of the N-oxide complex is greater than that for the pyridine complex. A decrease in the transition temperature, T_c, is expected from the known decrease in the sigma donor and increase in π donor abilities of the O atom in pyridine N-oxide compared to the N atom in pyridine. The effect of these changes in donor atom characteristics is to lower the d orbital energy gap and, as shown in the introduction, T_c.

The second analog was made with the intention of changing the cooperativity of the phase transition by changing the strength of the cation/cation coupling by the anion, by means of replacing BPh_4^- with the smaller anion PF_6^- (anion radius decreases from 3.30 Å to 3.06 Å respectively). This also resulted in an increase in the room temperature magnetic moment. However, until the full f_H vs T curve is determined for each compound, the reason for the increase in μ with PF_6^- cannot be given. Of the nine possibilities derived from $\Delta T_c > 0, = 0, < 0$

and $\Delta\Gamma > 0$, $= 0$, < 0 only four are consistent with an increased μ: $\Delta T_c = 0$, $\Delta\Gamma > 0$ and $\Delta T_c < 0$, $\Delta\Gamma < 0$, $= 0$ and > 0. If one assumes that T_c is more sensitive to Γ_H than Γ_S in

$$T_c = (\Delta H + \Gamma_H)/(\Delta S + \Gamma_S) \qquad (17)$$

then $\Delta T_c = \Delta\Gamma H/\Delta S$ and, given $\Delta S > 0$, ΔT_c has the same sign as $\Delta\Gamma$. Of the four possibilities for our result, only $\Delta T_c < 0$, $\Delta\Gamma < 0$ survives; it is expected, however, that T_c is less sensitive to Γ than is the slope of the f_Q/T curve, so that ΔT_c could be undeterminedly small. In that case $\Delta T_c \gtrsim 0$, $\Delta\Gamma > 0$ survives. In conclusion, the most direct interpretation of our results is that $\Delta\Gamma > 0, \Delta T_c \sim 0$ or that $\Delta\Gamma < 0$, $\Delta T_c < 0$.

One would like to relate the sign of $\Delta\Gamma$ to the cation/anion packing in the unit cell. While the X = 4Me-py, A = BPh_4^- salt structure is known[46] to be monoclinic P, the atom coordinate information was not reported. Further, the crystal structure of the PF_6^- salt is not known. At this juncture, all that can be said is that for the same Bravais lattice the replacement of a large anion with a small anion will cause cell contraction. This, in the most simple view, would lead to greater cooperativity in the phase transition by virtue of the cation volume change being a

larger fraction of the unit cell volume of the low spin phase. Whether this simple view is to be discarded must await a detailed inspection of crystal data for features of the cation/anion contacts.

The third analogs make use of the following substituents and anions; X = 3Me-py, 3,4Me-py, NA or DPA and A = BPh_4^- or Cl^-. The first modification in this group of compounds was to replace 3Me-py and 3,4Me-py with electron donating methyl groups on the pyridine by the corresponding carboxcylic acid, NA or DPA, respectively, with electron withdrawing carboxcylic groups. The electron withdrawal should lower the electron donating ability of the N atom, resulting in a reduction of the d orbit splitting and, again, a lower T_c and higher magnetic moment. For both modifications the magnetic results are as expected.

Before attempting to interpret the ESR data, let us first consider the theoretical resonance values for Fe(III). Normally, six coordinated low-spin Fe(III) exhibits an anisotropic g factor of about 2. In the case of large scale rhombic distortion of octahedral (O_h) symetry (g = 0), g rises to about 2. Due to this, we expect to see a resonance at $g \sim 2$ for our compounds with $f_Q < 1.0$ (see Table II). High-spin Fe(III) can give 1 to 5 resonance lines depending on the extent of distortion from O_h symmetry, as shown below:

O_h	(D, E = 0)	1 isotropic line g$\sim$2
C_4	(D<<hν, E=0)	5 lines
C_4	(D>>hν, E=0)	1 anisotropic line; g$\sim$2,6
C_2	(D, E $\neq$ 0)	1 isotropic line, g$\sim$4; 2 anisotropic lines g$\sim$1-10

The ESR spectra are not trivial to fully interpret and even appear to contradict the magnetic susceptability data regarding the extent of intersystem crossing in our complexes. Our complexes all fall into the C_2 catagory. The difficulties arise with the consistant observation of a resonance line at g$\sim$2. For two compounds, X = Cl^- or NA, which are magnetically pure high-spin, the resonance at g$\sim$2 means it is possible for the high-spin ion to give a resonance at this g. From these spectra we can state that while a g$\sim$4 resonance unequivocally demonstrates the presence of high-spin Fe(III), a g$\sim$2 resonance does not unambiguously charactize low-spin Fe(III) and can result from a superposition of low and high-spin site resonances as well as from high-spin alone. Furthermore, the intensity of this resonance may exceed that at g$\sim$4 and this can not be taken to mean $f_H < 0.5$. Consequently, we find no basis for disagreement in interpretation of the μ_{eff} and g values regarding the

values of f_H for our complexes.

Further evidence of anion size affecting the degree of cooperation comes from the cases where X = NA or DPA and A = BPh_4^- or Cl^-. In these cases, as the size of the anion decreases (3.30 Å to 1.8 Å), the magnetic moment increases and the g ~2, resonance line increases in magnitude. (These results are supported by work on an unrelated compound, and in which BPh_4^- and Cl^- were used as counterions. This work was discovered subsequent to our measurements.)[54]

Before discussing the Mossbauer spectrum of the samples it should be stated that the instrument was functioning at acceptable levels. As shown in Figure 18 (a baseline corrected baseline spectrum), the noise level of the spectrometer approaches the random level $\sigma = 1/\sqrt{N}$. Although the scatter may appear large on the scale used, most of the points fall within the ± 0.5 % theoretical limit of random noise.

As for the quality of the transmission spectrum of a standard, stainless steel foil, the signal:noise ratio is about 23:1. For the conversion electron spectrum of the same standard the signal:noise ratio is about 9:1. It was expected that the conversion electron spectrum would have a lower noise level but this was not the case, for an as yet unknown reason. Further investigations are required to resolve this.

Another problem that arose with the conversion electron detector was its failure to obtain a conversion electron spectrum of the Fe(III) salts. The problem is most likely due to a low sample density (low areal density of ^{57}Fe) of the samples.

Only one set of variable temperature transmission spectra has been presented for an equivelant compound, that of $[Fe(4Me\text{-}py)L]BPh_4$.[46] As with our spectra, the room temperature spectrum of the 4Me-py complex is characterized by a relatively small signal level, about 1 % absorption. While this is about 3 to 4 times smaller than the % absorption of our spectrum, the literature spectrum has a lower noise level. At temperatures in the spin transition range both spectra exhibit only a doublet, a not uncommon circumstance for mixed spin-state Fe(III) samples. Two possible explainations exist for this. The first is that, due to similar quadrapole splittings and center shifts, the absorption peaks for the high and low-spin sites overlap to the extent that they appear as a single doublet; this is unlikely. The second explaination is that the spin transition occurs on a time scale faster than that of the lifetime of the excited Mossbauer nuclear state (1×10^{-7} sec), leading to a time averaged spectrum.

The implications of this finding for our goal of studying surface spin-state distributions are as

follows. A "fast exchange" spectrum of Fe(III) is that of a weighted average of the low and high-spin state centershifts and quadrapole splittings. The weighted average spectrum for the surface sites will then show a different center shift and quadrapole splitting than do the bulk sites, with the change in these parameters revealing the change in the ratio of high:low-spin sites at the surface. To be quantitative about the change in distribution one must observe the CEMS at both the high and low temperature limits, so as to obtain the spectra of the pure high and pure low-spin surface species.

CONCLUSIONS

Several new compounds of the form [Fe(X)L]A were synthesized and were found to magnetically behave as expected. The transmission Mossbauer spectra for these compounds shows a time averaged doublet of the high and low-spin fractions. Other similar compounds have shown this behavior.[46,58-60] Although the relative amounts of high and low-spin species is not directly determinable from the spectra, the ratio can be calculated once the quadrapole splitting of the low-spin, from a liquid nitrogen temperature spectrum, and the high-spin fraction, from an elavated temperature spectrum, have been obtained. This can be easily calculated, as the quadrapole splitting of the time averaged spectrum is directly related to the fraction of each species present.

As for the conversion electron experiment, problems due to the areal density and surface charging of the sample seem to prevent the acquisition of good spectra. However, for the present system these problems may be overcome with the use of silver paint, to alleviate the surface charging, and by enrichment of the samples with ^{57}Fe, to partially offset the low areal density. Another possible, and perhaps better, method of conducting this experiment would be to use a hemispherical analyzer to capture the ejected electrons.

This offers many possibilities including the capacity for variable temperature studies. Furthermore, although the initial cost of the hemisphere may be high, the savings in the cost of the detector gas will soon be evident.

FUTURE DEVLOPMENT

The work presented in this manuscript can be developed further in three principle ways: ligand variation, anion variation and variable temperature studies of μ.

One area of ligand variation would consist of changing the ligand X=py by substituting electron donating groups, such as OR, OH, NH_2 or NR_2, in place of an H atom in the pyridine ring. This should tend to increase the electron density in the ring, due to an inductive donation from the substituents, and thus, increase of the degree of electron donation to the iron(III) center. Furthermore, if this increase in electron donation occurs primarily through the N atom lone pair (rather than through the π system) the complex should undergo a spin transition at a higher temperature due to an increase in the d orbital energy gap.

A second ligand modification of the pyridine ring would be to convert the substituted pyridine ligands to the corresponding N-oxides, as detailed by Shaw.[55] This should result in shifting the transition temperature to a lower value due to the lower σ donor and higher π donor abilities of the N-oxide ligand.

A third possible ligand variation would be to develop a new series of complexes by replacing the pyridine ligand with another ligand of the hetero-

aromatic type such as primidine or thiophene.

As for anion variation, to date only BPh_4^-, PF_6^- and Cl^- have been used as counterions. A study of the effect that the counterion has on the intersystem crossing temperature and cooperativity could prove interesting in itself and even more significant in comparison with the results of studies[56,57] on other intersystem crossing compounds. Suggestions for anions to be used include: SCN^-, ClO_4^-, NO_3^-, BF_4^-, and I^-.

Another avenue to more fully develop is a variable temperature study of the magnetic moments (μeff) and Mossbauer spectra of the compounds already prepared and of any new compounds.

Finally, it would be beneficial to prepare the materials in this study using enriched ^{57}Fe so that the differences in the surface and bulk site Mossbauer spectra can be better delineated by enhancing the signal:noise ratio.

REFERENCES

1. Gütlich, P. In Mössbauer Spectroscopy Applied to Inorganic Chemistry 1; Long, G. J., Ed.; Plenum: New York, 1984; Chapter 11.
2. Purcell, K. F.; Edwards, M. P. Inorg. Chem. 1984, 23, 2620.
3. Renovitch, G. A.; Baker, W. A. Jr. J. Am. Chem. Soc. 1967, 89, 6377.
4. König, E.; Madeja, K. Inorg. Chem. 1967, 6, 48.
5. Gütlich, P. Structure and Bonding 1981, 44, 83.
6. Sorai, M.; Seki, S. J. Phys. Chem. Solids. 1974, 35, 555.
7. Sorai, M.; Seki, S. J. Phys. Soc. Japan. 1972, 33, 575.
8. Hoseltun, M. A.; Wilson, L. J.; Drago, R. S. J. Am. Chem. Soc. 1975, 97, 1722.
9. Phillips, W. D.; Poe, M. Methods of Enzymol. 1972, 24, 304.
10. Evans, D. F. J. Chem. Soc. A. 1959, 2003.
11. Christian, J. W. The Theory of Transformations in Metals and Alloys; Pergamon: Oxford, 1965; pp 1, 224, 306, 410-425.
12. Rao, C. N. R.; Rao, K. J. Phase Transitions in Solids; McGraw-Hill: New York, 1978; pp 1, 68, 87.

13. Mikami, M.; Konno, M.; Saito, Y. Chem. Phys. Lett. 1979, 63, 566.

14. Beattie, J. K.; Binstead, R. A.; West, R. J. J. Am. Chem. Soc. 1978, 100, 3044.

15. Gütlich, P. In Chemical Mössbauer Spectoscopy; Herber, R. H. Ed.; Plenum: New York, 1984; chapter 2.

16. Mikami, M.; Konno, M.; Saito, Y. Chem. Phys. Lett. 1979, 63, 566.

17. Köppen, H.; Müller, E. W.; Köhler, C. P.; Spiering, H.; Meissner, E.; Gütlich, P. Chem. Phys. Lett. 1982, 91, 348.

18. Meissner, E.; Köppen, H.; Spiering, H.; Gütlich, P. Chem. Phys. Lett. 1983, 95, 163.

19. Gütlich, P. In Mössbauer Spectroscopy and Its Chemical Applications; Comstock, M. J. Ed.; Advances in Chemistry 194; American Chemical Society: Washington, DC, 1981, chapter 6.

20. Russel, K. C. In Phase Transformations; American Society for Metals: Metals Park, 1970, chapter 6.

21. Slichter, C. P.; Drickamer, H. G. J. Chem. Phys. 1972, 56, 2142.

22. Spiering, H.; Meissner, E.; Köppen, H. Müller, E. W.; Gütlich, P. Chem. Phys. 1982, 68, 65.

23. Ganguli, P.; Gütlich, P. J. Chem. Soc., Dalton Trans. 1981, 441.

24. Ganguli, P.; Gütlich, P.; Müller, E. W. Inorg. Chem. 1978, 21, 3429.

25. Gütlich, P.; Link, R.; Steinhaüser, H. G. Inorg. Chem. 1978, 17, 2509.

26. Sinn, E.; Sim. G.; Dose, E. V.; Tweedle, M.; Wilson, L. J. J. Am. Chem. Soc. 1978, 100, 3375.

27. Casey, A. T.; Isaac, F. Aust. J. Chem. 1967, 20, 2765.

28. Casey, A. T. Aust. J. Chem. 1968, 21, 2291.

29. Baker, W. A. Jr.; Bobonich, H. M. Inorg. Chem. 1964, 3, 1184.

30. Haddad, M. S.; Federer, W. D.; Lynch, M. W.; Hendrickson, D. N. J. Am. Chem. Soc. 1980, 102, 1468.

31. Haddad, M. S.; Federer, W. D.; Lynch, M. W.; Hendrickson, D. N. Inorg. Chem. 1981, 20, 131.

32. Tricker, M. J. In Mössbauer Spectroscopy and Its Chemical Applications; Comstock, M. J. Ed.; Advances in Chemistry 194; American Chemical Society: Washington, DC, 1981, chapter 3.

33. Debrunner, P. G.; Frauenfelder, H. In An Introduction to Mössbauer Spectroscopy; May, L. Ed.; Plenum: New York, 1971, chapter 1.

34. Swason, K. R.; Spijkerman, J. J. Appl. Phys. 1970, 41, 3155.

35. Jaggi, N. K.; Rao, K. R. P. M.; Dande, Y. D. Proc. Nucl. Phys. Solid State Phys. Symp. 1981 1982, 24c, 557.

36. Berry, F. J. T. Metal Chem. 1979, 4, 209.

37. Cranshaw, T. E. J. Phys. E: Sci. Instrum. 1974, 7, 122.

38. Dunham, W. R.; Wu, C. T.; Polichar, R. M.; Sands, R. H.; Harding, L. J. Nucl. Instrum. Methods 1977, 145, 537.

39. Lang, G.; Dale, B. W. Nucl. Instrum. Methods 1974, 116, 567.

40. Ruebenbauer, K.; Birchall, T. Hyperfine Interactions 1979, 7, 125.

41. Nullens, H.; Roy, G. de; Espan, P. V; Adams, F.; Vansant, E. F. Anal. Chim. Acta. 1980, 122, 373.

42. Spijkerman, J. J. In An Introduction to Mössbauer Spectroscopy; May, L. Ed.; Plenum: New York, 1971, chapter 2.

43. Shigematsu, T.; Pfannes, H. -D.; Keune, W. In Mössbauer Spectroscopy and Its Chemical Applications; Comstock, M. J. Ed.; Advances in Chemistry 194; American Chemical Society: Washington, DC, 1981, chapter 6.

44. Fenyves, E.; Haiman, O. The Physical Principles of Nuclear Radiation Measurements; Academic: New York, 1969, pp 134-135.

45. Sorai, M.; Ensling, J.; Hasselbach, K. M.; Gütlich, P. Chem. Phys. 1977, 20, 197.

46. Matsumoto, N.; Ohto, S.; Yoshimura, C.; Ohyoshi, A.; Kohata, S.; Okawa, H.; Maeda, Y. J. Chem. Soc., Dalton Trans. 1985, 2575.

47. Black, G.; Depp, E.; Corson, B. B. J. Org. Chem. 1949, 14.

48. Sorai, M.; Ensling, J.; Gütlich, P. Chem. Phys. 1976, 18, 199.

49. Inorganic Syntheses Vol. V; Moeller, T. Ed.; McGraw-Hill: New York, 1957; pp 179-181.

50. Mulay, L. N.; Boudreaux, E. A. Theory and Applications of Molecular Diamagnetism; John Wiley and Sons: New York, 1976.

51. Nakamoto, K. Infrared and Raman Spectra of Inorganic and Coordination Compounds; Wiley-Interscience: New York, 1978.

52. Pouchert, C. J. The Aldrich Library of Infrared Spectra; Aldrich Chemical: Milwaukee, 1981.

53. Drago, R. S. Physical Methods in Chemistry; W. B. Saunders: Philadelphia, 1977.

54. Dosser, R. J.; Eilbeck, W. J.; Underhill, A. E.; Edwards, P. R.; Johnson, C. E. J. Chem. Soc. A. 1969, 810.

55. Shaw, E. N. In Pyridine and Derivatives, Part Two; Klingsberg, E. Ed.; Interscience: New York, 1961, chapter 4.

56. Sams, J. R.; Tsin, T. B. J. Chem. Soc. Dalton Trans. 1976, 488.

57. Sams, J. R.; Tsin, T. B. Inorg. Chem. 1976, 15, 1544.

58. Ohta, S.; Yoshimura, C.; Matsumoto, N.; Okawa, H.; Ohyoshi, A. Bull. Chem. Soc. Jpn. 1986, 1, 155.

59. Ohyoshi, A.; Honbo, J.; Matsumoto, N.; Ohta, S.; Sakamoto, S. Bull. Chem. Soc. Jpn. 1986, 5, 1611.

60. Maeda, Y.; Takashima, Y.; Matsumoto, N.; Ohyoshi, A. J. Chem. Soc. Dalton Trans. 1986, 1115.

AN INVESTIGATION INTO THE MAGNETIC PROPERTIES ASSOCIATED WITH THE SPIN CROSSOVER OF Fe(III) COMPOUNDS OF THE FORM [Fe(X)L]A

by

Thomas J. Jewett
B. S., Loras College, 1984

AN ABSTRACT OF A MASTER'S THESIS

submitted in partial fulfillment of the
requirements for the degree

MASTER OF SCIENCE

Department of Chemistry

KANSAS STATE UNIVERSITY

Manhattan, Kansas

1987

Abstract

The magnetic behavior of compounds of the form [Fe(X)L]A, where x = pyridine or a substituted derivative and A = BPh_4^-, PF_6^- or Cl^-, was studied for the purpose of determining where the transition from low to high-spin preferentially initiates. Included in this study were several new compounds which were synthesized then characterized by magnetic susceptibility and esr measurements; they were found to magnetically behave as expected. In considering the sites of preferential initiation of the transition, thermodynamics predict that the surface, in particular corners and edges, should provide the sites where the transition initiates. It was desired to test this prediction using transmission Mossbauer and conversion electron Mossbauer spectroscopy,respectively a bulk and a surface technique. However, due to a problem with the areal density of ^{57}Fe in the prepared crystalline samples, conversion electron spectra of the compounds could not be obtained. Transmission spectra were obtained from packed samples and appear as time averaged spectra of the two magnetic phases. This results since the spin transition occurs on a time scale faster than the lifetime of the excited Mossbauer nuclear state, (1×10^{-7} sec). The doublet can be analyzed in terms of its weighted average of low and high spin components once liquid nitrogen and elavated transmission spectra have been obtained. As for the problem with the conversion electron detector, use of enriched samples should overcome the areal density problem.